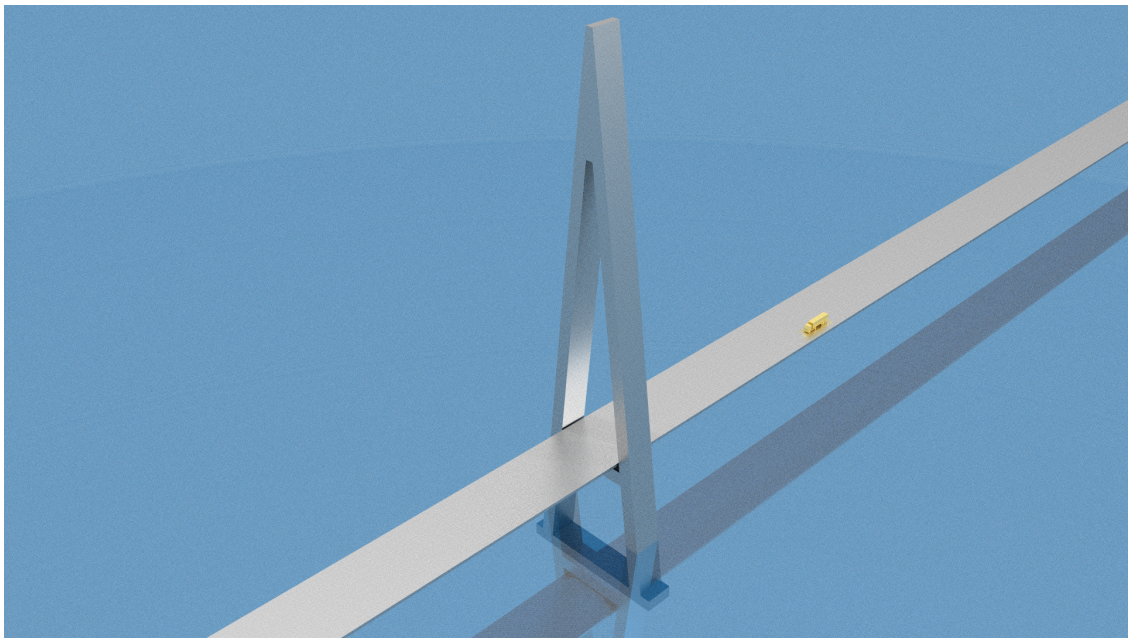

Aerodynamic Investigations of Vehicles under High Side Wind Conditions on Bridges

Master thesis in Applied Mechanics
Master thesis in Automotive Engineering

Wei Wang

Sriprasanna Venkatesh Hariharan

Department of Mechanics and Maritime Sciences

CHALMERS UNIVERSITY OF TECHNOLOGY
Gothenburg, Sweden 2021
www.chalmers.se

Master Thesis in Applied Mechanics
Master Thesis in Automotive Engineering

Aerodynamic Investigations of Vehicles under High Side Wind Conditions on Bridge

Sriprasanna Venkatesh Hariharan
Wei Wang

CHALMERS
UNIVERSITY OF TECHNOLOGY

Department of Mechanics and Maritime Sciences
Division of Vehicle Engineering and Autonomous Systems
Chalmers University of Technology
Gothenburg, Sweden 2021

Aerodynamic Investigations of Vehicles under High side Wind Conditions on Bridges
Sriprasanna Venkatesh Hariharan
Wei Wang

Supervisor: Alexey Vdovin, Department of Mechanics and Maritime Sciences
Examiner: Alexey Vdovin, Department of Mechanics and Maritime Sciences

Report Number: 2021: 41
Master's Thesis 2021
Department of Mechanics and Maritime Sciences
Division of Vehicle Engineering and Autonomous Systems
Chalmers University of Technology
SE-412 96 Gothenburg
Telephone +46 31 772 1000

Typeset in LaTeX
Printed by Chalmers Reproservice
Gothenburg, Sweden 2021

Aerodynamic Investigations of Vehicles under High Side Wind Conditions on Bridges
Sriprasanna Venkatesh Hariharan
Wei Wang
Department of Mechanical Engineering
Chalmers University of Technology

Abstract

Crosswind stability is a critical safety factor that needs to be addressed for all types of road vehicles. However, it is especially crucial for trucks and buses due to their large lateral areas. As a result, this makes the vehicles more vulnerable to high side forces caused by incoming side winds. This is because of the fact that, the greater the lateral area, the greater the sensitivity to side winds. In the absence of any shielding, the magnitude of the resulting side force on the vehicles commuting across the bridge will be exacerbated. In addition to side force, the yaw moment acting on the truck is also an important factor that needs to be addressed. The lateral stability of the vehicle is mainly affected by yaw moments. When side winds blow, the presence of a bridge structure, such as a pylon, causes huge turbulent wake flows due to flow separation. Furthermore, when the vehicle rides across the pylon wake, the sudden shielding effect in the wake flow region causes a steep change in the vehicle's side force. The pressure distribution on the surface of the vehicles as well have continuous variation and thus result in fluctuating yaw moments. These disturbances have an impact on the drivability and maneuverability of the vehicle. Handling stability is extremely important for road safety. If these side wind sensitive vehicles are traveling at high speeds, it may even cause them to roll over in severe cases. So, it is pivotal to analyze the side wind induced aerodynamic forces and moments on road vehicles in order to understand their impact and to provide guidance to drivers on how to maintain the vehicle's stability when driving in this scenario.

The road vehicle taken for this study is a truck. 3D Computational Fluid Dynamics (CFD) simulations are performed to investigate the aerodynamic forces and moments on the truck at different side-wind conditions. The commercial code used to simulate the model is the StarCCM+. Initially, a steady state case is developed and solved using Reynolds Averaged Navier Stokes($RANS$) transport equations and a realizable $k-epsilon$ turbulence model with all necessary boundary conditions. The aerodynamic coefficients of the truck are computed at different positions on the bridge. Individual and combined effects of bridge structures such as deck, windshield, and pylon are investigated. Unsteady simulations are also performed, and the results are compared to the steady-state model. The steady state results are used as an initial solution for the unsteady model. The unsteady model is built to simulate the motion of a truck across the bridge by using overset mesh methodology. The simulations are run for 30, 60 and 90 degree yaw conditions. The CFD investigations showed that the presence of deck and windshield(non-porous and solid) reduces the side force acting on the truck by diverting the flow above with a local re-circulation wake region beside the exposed windward surface, and thus reduces the static pressure on the truck. On the other hand, the porous windshields increase the side force on truck when compared against the windshields with no cut-outs. The study on porous windshields revealed an intriguing scenario in which the presence of windshields with more than 80% porosity increases the side force on the truck when compared to the case with no shields.

Keywords: Aerodynamics, Side wind effects, CFD, Overset mesh, Unsteady simulation

Preface

This study has been done as a part of master thesis work at the department of Mechanics and Maritime Sciences in Chalmers University of Technology. This thesis has been carried out under the supervision of Dr. Alexey Vdovin (Researcher at Mechanics and Maritime Sciences, division of Vehicle Engineering and Autonomous Systems Group in Chalmers University of Technology) with the stakeholders of the Norwegian Public Roads Administration (NPRA). This thesis is examined by Dr. Alexey Vdovin.

Acknowledgements

First of all, we would like to express our sincerest gratitude to Dr. Alexey Vdovin for having believed in our abilities and offered this project work for writing our master's thesis under his supervision. We would as well like to thank from the bottom of our heart for his continued support, guidance, supervision and encouragement throughout the thesis work. Despite this extraordinary situation of an outbreak of a pandemic, he has conducted regular meetings and provided his valuable feedback on the progress and directed with key data and inputs to achieve the primary goal and deliverable of this project. He has also provided many supporting literature that are in close connection with this topic, tutorials on the StarCCM+ commercial code to get hands-on experience, lectures on Linux platform and cluster for running simulations and also the truck model for which the CFD investigations are carried out.

Sriprasanna Venkatesh Hariharan, Wei Wang
Gothenburg, June 2021

Contents

List of Figures

List of Tables

1

Introduction

1.1 Background

The Norwegian Public Roads Administration (NPRA) is focused on investigating the effects of harsh side winds on vehicles passing over floating bridges. This comprises the effects of bridge structures like deck, pylon, and windshields. The primary goal is to comprehend the effects of wind-induced side forces and moments on trucks as they travel across bridge pylons. The floating bridge itself is sensitive to high side winds due to its large surface area and as well subjected to additional loads from the waves.

Therefore, if the design of the bridge structure is not optimized, then it will need to have concerns about its structural integrity, which is purely wind-induced. So, the bridges are built with a minimal area of exposure to the wind. As a result, vehicles traveling on the bridge are less protected from side winds, and the effects of side forces are more prominent. What is more, the bridge is designed to be a floating bridge. The additional forces from the waves will also increase the instability.

In general, road vehicles with large side areas are more vulnerable to crosswinds and more prone to roll-over, thus possess high lateral instability than passenger vehicles [1]. There have been a few discussions about vehicles commuting over floating bridges when there are predictions of strong winds. As well, the bridge structures like pylon, generate large turbulent wake flows and induce high yaw moments on the truck as it passes across. Due to the heavy side winds that could occur, the NPRA focuses on giving recommendations on the optimal speed for vehicles with large side areas that commute on the bridge or if the bridge should be closed for these vehicles if the conditions are too harsh. In this case, the side force investigations are vital to provide necessary recommendations. Crosswind stability is an important safety concern for manufacturers of different types of road vehicles (passenger cars, vans, buses and trucks etc.). The influence of the crosswind on the larger side-area road vehicles, such as trucks, has become more sensitive. A truck in motion is subjected to different aerodynamic forces such as drag, lift, side force and aerodynamic moments such as yaw, roll and pitch moments. These forces and moments depend basically on the wind's relative velocity and relative direction (yaw) to the truck's motion. In the case of a strong side wind, the side force and lift force might lead the truck to end up in a lane departure or overturn. Hence, in this study, the focus is on investigation of the resulting forces from the side wind that acts on a truck, as well as understanding its dynamic influence on a moving truck.

1.2 Objective Statement

The thesis is centered on side wind investigations, with a primary emphasis on:

- To perform CFD simulations and to investigate the effects of bridge structures (Deck, Pylon and Windshields) on the aerodynamic forces and moments acting on the truck.
- To compare and differentiate the individual effect of bridge structures versus the combined effect on aerodynamic forces.
- To simulate, investigate and to compare the effect of solid (non-porous) versus porous windshields or wind-barriers on the bridge deck.
- To study the effect of windshield height and wind guides on resulting forces on trucks.
- To conduct unsteady CFD investigations for truck movement across the wake of the bridge pylon using a moving mesh strategy and compare it to steady state simulations.

1.3 Limitations

It is a well-known fact that the simulations models are always a simplification from the actual physics. The CFD models have few limitations in terms of mimicking the real-world scenarios. One of the main concerns is, for high side-wind case of 90yaw, the velocity inlet magnitude in the direction of truck motion is zero. This is because, as with 90 yaw side wind, the cosine component in the i direction (x) is zero when resolved. As a result, there is only the $j$component (y). In this case, the main velocity inlet will be from the side (perpendicular to the truck). This scenario has the effect of causing the vehicle to have a negative drag coefficient when it is in the wake region. This is physical, but with the only exception that the truck's movement is not captured.

As the CFD simulations are performed with bridge structures, it needs to be evaluated with the experimental results from wind tunnel tests for the purpose of estimating the accuracy and as well to calibrate the CFD model. But to carry out such physical tests, construction and mounting of the bridge deck, pylon and windshields along with the truck inside the wind tunnel needs to be done. This process is quite complex in terms of having an appropriate physical model size of bridge structures, mounting and accessibility parameters in the wind tunnels.

As the domain is quite big for this study, the best mesh configuration is composed of 100 million cells as this is a 3D simulation. Hence, the model is computationally expensive as well as time consuming to solve the case.

2

Theory and Background

2.1 Fluid Dynamics and Continuum

Fluid dynamics deals with the study of fluids in motion and computational fluid dynamics is the numerical analysis of fluid flow which solves the flow-field properties in the computational domain. The fluid in motion can be liquid, gas or a combination of both in some cases. But for external vehicle aerodynamics, the fluid generally preferred for CFD investigations is air with constant density i.e; incompressible medium. The matter is made up of discrete molecules and the density with which they are packed defines its state. Fluid state has particles with relatively low density as compared to solids. The particles in fluids are in a state of random motion and thus always colliding with each other. However, for general engineering problems, the matter is not studied in such microscopic scales instead they are visualized and studied in a more macroscopic level known as continuum. In continuum, the length and time scales of the matter are larger than the microscopic scales and mesoscales. The approach used in this study is a continuum approach by numerically solving Navier-Stokes(NS) transport equations. These transport equations typically represent the flow in terms of field properties such as pressure, density, temperature and flow velocity etc. as functions of space and time(transient/unsteady).

2.2 Governing Equations

The Navier-Stokes(NS) equations are a set of partial differential equations which basically consists of the continuity equation (mass conservation) and momentum conservation equations.

2.2.1 Continuity Equation

The continuity or the mass conservation equation states that the net rate of mass flow into the control volume is same as the net rate of mass outflow from the control volume, and thus representing the mass flow conservation.

$$\frac{\partial \rho}{\partial t} + \frac{\partial \rho v_i}{\partial x_i} = 0 \tag{2.1}$$

The first term in the eqn.2.1 is the unsteady term and it represents the change in fluid density with time. The second term i.e; the convective term is the spatial change of mass flow across the boundaries. Usually for incompressible flows, the first term will not be accounted as the density is constant. Then the eqn.2.1 can be expressed as,

$$\frac{\partial v_i}{\partial x_i} = 0 \tag{2.2}$$

2.2.2 Momentum Equation

The NS momentum conservation equation states that the rate of change of momentum equals the net forces acting on the fluid.

$$\rho \frac{dv_i}{dt} = -\frac{\partial P}{\partial x_i} + \frac{\partial \tau_{ij}}{\partial x_j} + \rho f_i \tag{2.3}$$

The first term in the LHS of eqn.2.3 is the total derivative of field velocity. In general, it is given as,

$$\frac{dv_i}{dt} = \frac{\partial v_i}{\partial t} + \frac{\partial v_i v_j}{\partial x_j} \tag{2.4}$$

This term is the convective term in NS momentum equation, and it is responsible for the transport of flow-fields in all dimensions.

The first term in the RHS of eqn.2.3 is the gradient of pressure which acts as a source term. The second term is the gradient of stresses acting on the fluid element and the last term represents the body forces acting on the fluid like gravity, buoyancy etc.

For the incompressible flow with constant dynamic viscosity μ, the eqn.2.3 can be re-written as,

$$\rho \frac{dv_i}{dt} = -\frac{\partial P}{\partial x_i} + \mu \frac{\partial^2 v_i}{\partial x_j \partial x_j} + \rho f_i \tag{2.5}$$

2.2.3 Energy Equation

The energy conservation equation is deduced from the first law of thermodynamics, which states that the rate of change of energy in a control volume is equal to the sum of rate of heat added and the rate of work done. The Energy conservation equation is given as,

$$\rho c_p \frac{dT}{dt} = \Phi + \frac{\partial}{\partial x_i}\left(k \frac{\partial T}{\partial x_i}\right) + \rho z \tag{2.6}$$

where c_p is the specific heat capacity constant, T is the temperature, k is the heat conductivity constant and z is the net radiative heat source.

The term-1 in the LHS of eqn.2.6 signifies the internal energy of the system. The term-1 in the RHS indicates the viscous dissipation phenomenon which represents the conversion of kinetic energy to thermal energy. The term-2 on RHS denotes the heat flux and term-3 denotes the radiative phenomenon.

2.2.4 Reynolds-Averaged Navier-Stokes Equations

The steady-state Reynolds-averaged Navier–Stokes (RANS) equations are solved using the SIMPLE algorithm for pressure–velocity coupling. Discretization is performed using the finite-volume method with a second-order upwind scheme for all variables. The steady sate $RANS$ equation is given as

$$\rho\frac{\partial\bar{v}_i\bar{v}_j}{\partial x_j} = -\frac{\partial\bar{p}}{\partial x_i} + \frac{\partial}{\partial x_j}\left(\mu\frac{\partial\bar{v}_i}{\partial x_j} - \rho\overline{v_i'v_j'}\right) \tag{2.7}$$

Almost majority of fluid flows are turbulent, that is, three-dimensional and transient. Due to this chaotic random behavior, the fluid flow will experience turbulent fluctuations, means that the pressure and velocity is defined as the sum of mean value and a perturbation term. The turbulent flow field is generally decomposed as

$$u_i = \bar{u}_i + u_i' \tag{2.8}$$

$$p = \bar{p} + p' \tag{2.9}$$

Where u_i and p represents the instantaneous value, $\bar{u}_i$ and $\bar{p}$ denotes the mean part, u_i' and p' denotes the fluctuating turbulent parts.

To handle this, the equations (continuity and momentum), with additional terms due to fluctuations are time averaged. The new equations are called as Unsteady Reynolds-Averaged Navier-Stokes equations, abbreviated as $URANS$. The $URANS$ equations for the momentum transport are given as,

$$\rho\frac{\partial\bar{u}}{\partial t} = -\frac{\partial\bar{p}}{\partial x} + \rho g_x + \frac{\partial}{\partial x}\left(\mu\frac{\partial\bar{u}}{\partial x} - \rho\overline{u'^2}\right) + \frac{\partial}{\partial y}\left(\mu\frac{\partial\bar{u}}{\partial y} - \rho\overline{u'v'}\right) + \frac{\partial}{\partial z}\left(\mu\frac{\partial\bar{u}}{\partial z} - \rho\overline{u'w'}\right) \tag{2.10}$$

$$\rho\frac{\partial\bar{v}}{\partial t} = -\frac{\partial\bar{p}}{\partial y} + \rho g_y + \frac{\partial}{\partial x}\left(\mu\frac{\partial\bar{v}}{\partial x} - \rho\overline{u'v'}\right) + \frac{\partial}{\partial y}\left(\mu\frac{\partial\bar{v}}{\partial y} - \rho\overline{v'^2}\right) + \frac{\partial}{\partial z}\left(\mu\frac{\partial\bar{v}}{\partial z} - \rho\overline{v'w'}\right) \tag{2.11}$$

$$\rho\frac{\partial\bar{w}}{\partial t} = -\frac{\partial\bar{p}}{\partial z} + \rho g_z + \frac{\partial}{\partial x}\left(\mu\frac{\partial\bar{w}}{\partial x} - \rho\overline{u'w'}\right) + \frac{\partial}{\partial y}\left(\mu\frac{\partial\bar{w}}{\partial y} - \rho\overline{v'w'}\right) + \frac{\partial}{\partial z}\left(\mu\frac{\partial\bar{w}}{\partial z} - \rho\overline{w'^2}\right) \tag{2.12}$$

The eqn.2.10, 2.11 and 2.12 represents the $RANS$ momentum equation for the transport of the field property in x-direction, y-direction and z-direction.

2.3 Turbulence modelling

The irregular, chaotic and random movement of the mean flow is characterized as the turbulent flow. In this study, $RANS$ k - ϵ turbulence model is used to model the turbulent flow for the closure of $RANS$ equations and as well to model the flow-field in the computational domain. The k - ϵ turbulence model is a two-equation model, which solves the transport equation for turbulent kinetic energy k and turbulent dissipation rate ϵ. These two parameters determine the turbulent length scale and turbulent viscosity of the fluid. The turbulent length scale and the turbulent viscosity is given by,

$$l = \frac{k^{\frac{3}{2}}}{\epsilon} \tag{2.13}$$

$$\nu_t = c_\mu k^{\frac{1}{2}} l \tag{2.14}$$

In addition to this, the realizable k - ϵ turbulence model is used to have all the normal stresses in the domain to stay positive. This is carried out by damping the coefficient C_μ using a function of mean flow and turbulent properties. The two-layer k - ϵ model approach models the turbulent dissipation rate ϵ and turbulent viscosity μ_t as the functions of wall distance in the near proximity to the wall. The turbulent kinetic energy(k) is computed numerically through the modelled k equation across the whole computational domain. The $RANS$ k - ϵ turbulence model is commonly used for the analysis of turbulent flows far away from the wall region. The eqn. 2.15, 2.16 and 2.17 describes the modelled k and ϵ equations.

$$v_t = C_\mu \frac{k^2}{\varepsilon} \tag{2.15}$$

$$\frac{\partial k}{\partial t} + u_j \frac{\partial k}{\partial x_j} = \frac{\partial}{\partial x_j}\left[\left(v + \frac{v_t}{\sigma_k}\right)\frac{\partial k}{\partial x_j}\right] + G - \varepsilon \tag{2.16}$$

$$\frac{\partial \varepsilon}{\partial t} + u_j \frac{\partial \varepsilon}{\partial x_j} = \frac{\partial}{\partial x_j}\left[\left(v + \frac{v_t}{\sigma_\varepsilon}\right)\frac{\partial \varepsilon}{\partial x_j}\right] + C_{\varepsilon 1}\frac{\varepsilon}{k}G - C_{\varepsilon 2}\frac{\varepsilon^2}{k} - \frac{f_\mu \eta^3 \left(1 - \eta/\eta_0\right)}{1 + \beta\eta^3}\frac{\varepsilon^2}{k} \tag{2.17}$$

2.4 Boundary Layer Theory

Close to the surface of the vehicle, the boundary layer develops as the viscosity becomes dominant. Boundary layer development is highly significant in the wall bounded flows, where there is a significant velocity gradient normal to the direction of the flow indicating the presence of viscous regime. First, the boundary layer is laminar near the wall region and after the flow has passed the laminar boundary layer thickness, the boundary layer becomes turbulent with a significant increase in the turbulent viscosity (μ_t). The transition is influenced by different factors such as the distance from the leading edge or the local pressure gradient. On a contrary to the laminar boundary layer, the turbulent boundary layer provokes more friction at the surface, and therefore, the friction drag is increased through its presence. However, the characteristics of the turbulent boundary layer delay the separation location, which in turn, influences the aerodynamic forces.

The non-dimensional wall y^+ is an appropriate factor to describe the boundary layer. It is a function of absolute distance from the wall and wall shear stress. It is given as,

$$y^+ = \frac{u_\tau y_N}{v} \tag{2.18}$$

where u_τ is the wall friction velocity and y_N is the normal distance from the wall surface. Different range of y^+ denotes the different flow regimes. It is usually divided into three

regimes i.e; viscous sub-layer, log layer and the buffer region. Viscous sub-layer is the region closer to the wall, where the viscous effects are most prominent. Log-layer will be found far away in the boundary layer. The buffer region exists between viscous sub-layer and log-law region. The viscous regime, where the wall unit y^+ is found to be in the range y^+<50, describes the large domination of viscous stresses. Moving more and more closer to the wall within this range, makes the viscous effects more significant. Resolving the boundary layer requires mesh points down to the viscous sublayer for a better accuracy. This is an important parameter to be considered in the computational mesh-grid design.

However, for any given case, the desired y^+ value depends on the turbulence model and suitable wall y^+ treatment models. In this study, it was decided to have the wall y^+ between 30 to 300 with few cells having y^+ <30 and few having y^+ >300 as per the recommendations on Simcenter Steve-portal guide.

2.5 Aerodynamics

Aerodynamics is the study of interaction of the fluid flow with the moving or stationary bodies. Aerodynamics is primarily concerned with the forces and moments caused by air passing over and around the interacting bodies. Three prime important forces that acts on a moving vehicle are the drag force, lift force and the side force. The drag force component acts in the opposite direction of vehicle's motion and acts as the resistance to desired vehicle speed and affects the vehicle's performance. Drag components are categorized as pressure drag and skin friction drag, where the former is the most dominant one in the case of typical road vehicles. Pressure drag is mainly observed in the bluff bodies while the viscous drag is associated with the streamlined bodies. The lift force acts in the direction perpendicular to the direction of vehicle motion. The pressure difference between the roof and underneath of the truck mainly influences this lift force. The non-dimensionalized drag and lift properties to represent their respective influence for a particular geometrical attribute of a vehicle under given ambient flow-field conditions are given as,

$$C_d = \frac{2 * F_x}{\rho * v^2 * A} \tag{2.19}$$

$$C_l = \frac{2 * F_z}{\rho * v^2 * A} \tag{2.20}$$

$$C_s = \frac{2 * F_y}{\rho * v^2 * A} \tag{2.21}$$

Where F_d and F_l denotes the drag and lift force, ρ is the density of the fluid (air in general), v is the free-stream velocity and A denotes the frontal area of the vehicle. The C_s, C_d and C_l denotes the side force, lift force and the drag force coefficients. The frontal area and the velocity are retained to be same for all the yaw angles. All the above-mentioned aerodynamic coefficients are mainly dependent on and influenced by the shape and design of the vehicle.

In a similar manner, the equations for the moment coefficients are given as,

$$C_{m_x} = \frac{2 * M_x}{\rho * v^2 * A * L} \tag{2.22}$$

$$C_{m_y} = \frac{2 * M_y}{\rho * v^2 * A * L} \tag{2.23}$$

$$C_{m_z} = \frac{2 * M_z}{\rho * v^2 * A * L} \tag{2.24}$$

The C_{m_x}, C_{m_y} and C_{m_z} denotes the roll moment, pitch moment and yaw moment respectively. The density(ρ) of air is considered at 25°C i.e. 1.184 kg/m3, the velocity for this case is taken as 100 kph, the frontal area of the truck ($10.01m^2$) and L denotes the total truck length of the model, which is 14.24 m. Fig.2.1 represents the aerodynamic forces and moments on the truck.

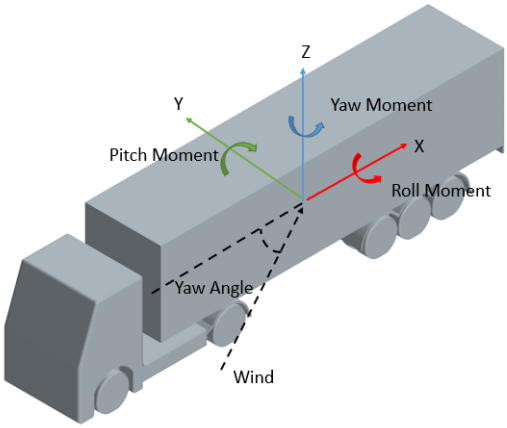

Figure 2.1: Aerodynamic forces and moments on the truck.

2.5.1 Fundamentals of Ground Vehicle Aerodynamics

Due to the low speed of the ground vehicles, the flow is assumed to be described by the incompressible Navier-Stokes (NS) equations as the change in density is considered to be insignificant. So, the equations 2.3, 2.10, 2.11 and 2.12 will be used for the numerical investigations of aerodynamic phenomenon. In these cases, typically, the Reynolds number (Re) considered is fairly high i.e; $2.7 * 10^6 < Re < 8 * 10^6$. On the frontal part of the vehicle the flow is first laminar with a stagnation region and then a transition to a turbulent flow occurs rapidly with the flow separation. The base area of a typical car, truck or bus are prone to a large turbulent wake that are more likely to be formed. Strong unsteady turbulent phenomena such as vortex shedding occurs in these wake regions. All these make fair challenges for the numerical simulations and a trade-off between the full representation of the model physics and the numerical resources to be used has to be made to effectively study the flow phenomenon over bluff bodies.

2.5.2 Crosswind Aerodynamics

A crosswind is characterized by the presence of perpendicular or inclined component of the flow to the direction of travel. The presence of this crosswind component will have significant effects on lateral displacement, lateral acceleration, yaw moment and the handling stability. However, the effects from the crosswinds are as well highly influenced by the incoming flow angle or the yaw angle, the relative speed and the crosswind strength. The worst case of high crosswind scenario would be the rollover of the vehicle which is more likely to be wind-induced. The crosswinds are generally non-uniform as the atmospheric boundary layer of the wind causes a sheared crosswind and as well transient/unsteady due to the presence of wind gusts and obstacles along the road side. The eqn.2.27 represents the transient effects on the resulting flow,

$$\frac{d\vec{u}_{\text{resultant}}}{dt} = \frac{\partial u_{vehicle}}{\partial t} + \frac{\partial \vec{u}_{\text{wind}}}{\partial t} + u_{vehicle}\frac{\partial \vec{u}_{\text{wind}}}{\partial x} \tag{2.25}$$

The first term on the RHS of the equation corresponds to vehicle acceleration, the second term corresponds to the variations of incoming wind in time(transient) and the last term corresponds to the influence of different wind conditions on driving. All these parameters will have the transient effects on the resulting flow.

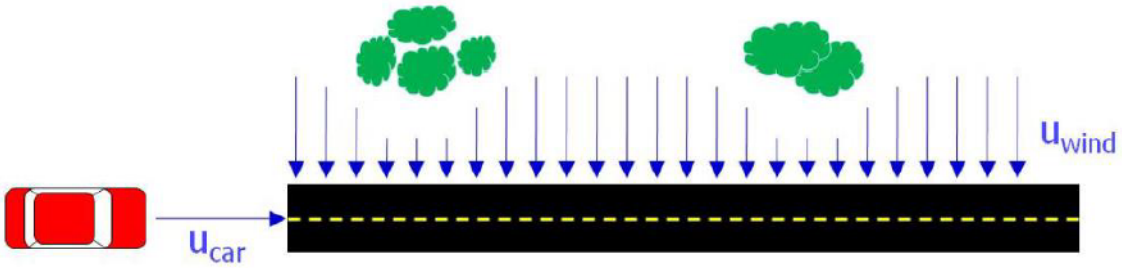

Figure 2.2: Transient effects on resulting flow.

The transient crosswinds are common sources of discomfort in the ground vehicles. Added to this, in order to reduce the fuel consumption, automobile manufacturers tend to develop lighter vehicles with drag reducing designs. As a consequence, the center of pressure is often moved forward and thus increasing the tendency to yaw when exposed to crosswinds. As well, increasing the power of the engines, allows the vehicle to travel at high speeds and causing it to be more sensitive to the unsteady crosswinds. Crosswind stability is the result of complex interactions between aerodynamics, vehicle dynamics and the driver. For trucks, the large lateral surface area of the trailer and variable road conditions, the handling stability of the vehicle under intense crosswind is very crucial for the road safety.

The unsteady effect of crosswind can play a role in the motion of vehicle itself. This can have two effects. The lateral velocity or the yaw rate of the vehicle can result in relative wind that influences the aerodynamics. Secondly, if the vehicle takes a large yaw motion, the crosswind will affect the vehicle with a modified angle ψ, and thus changes the aerodynamics around the vehicle. This is illustrated by the fig 2.3.

In this study, the aerodynamic effect of crosswinds on the vehicles moving over the bridges provided with deck and pylon, is studied and analyzed for different cases through CFD

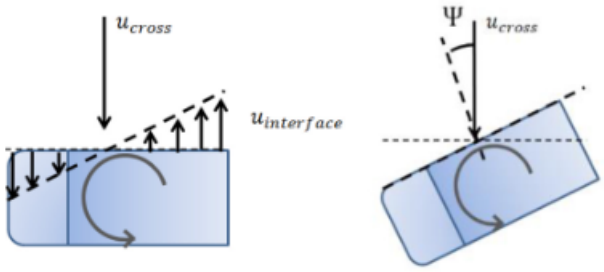

Figure 2.3: Effects of crosswind on vehicle motion.

simulations. The vehicles commuting on the bridges are not shielded from the incoming side wind i.e; the crosswinds that blows perpendicular to the direction of travel. As a result, the vehicles will be exposed to high side forces. In addition to this, the bridge pylon creates huge wake. The vehicles are prone to have high yaw moments, induced by harsh winds, as they travel across the accelerated flow regions of the pylon wake. The fig.2.4 represents the truck moving on a bridge with deck (road) and the vertical pillars called as pylon. This has an interesting aerodynamic effect with regard to side force C_s and yaw moments.

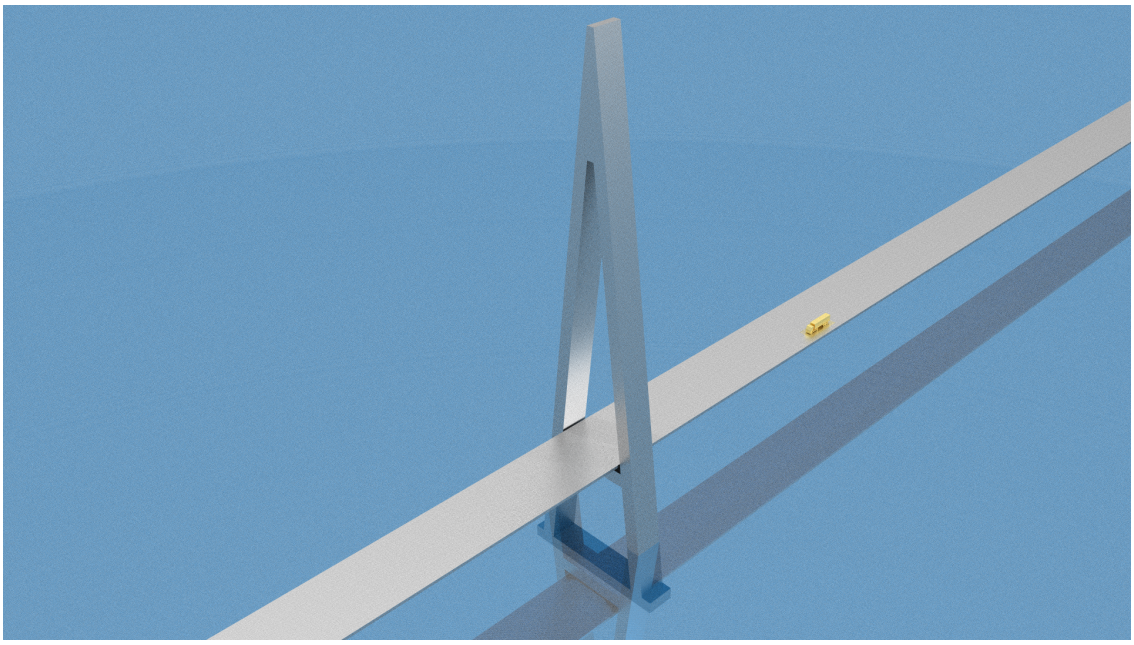

Figure 2.4: Truck on bridge deck with vertical pylon.

2.6 Literature Study

In L.Salati and P.Schito[2] work, it was found that the truck wake is developed in both the x- and y-directions according to the incoming yaw angle of crosswind and the vehicle speed. The pylon wake is mainly developed in the y-direction with two main vortices generated on the right and left-side of the pylon away from wake, which is responsible for increase of the side force acting on the truck when it passes through that region. It

was also observed that, the aerodynamics actions decrease, especially lateral force and yaw moment, in the close proximity of pylon due to the increase in the shielding effect on trucks from the incoming crosswinds. As the vehicle exits the pylon wake, it is then returned to the undisturbed constant values of aerodynamic force coefficients and the pressure distribution on the surface. Because of the crosswind angle acting on the vehicle, it was also shown the possibility to observe a positive pressure coefficient on the windward surface of the truck. As well, when the vehicle is in the wake of the pylon, a very low pressure value is observed. Also, L.Salati and P.Schito[2], concluded the findings with a remark that, the transient variation of pressure distribution on the vehicle surface from the cab(tractor) to the trailer determines the yawing moment that may be critical for the safety of heavy vehicles, and which may end-up in wind-induced rollover at high speeds.

T.Argentini and E.Ozkan[3] observed and highlighted the phenomenon of shielding effect from the bridge pylon. Due to the presence of shielding near the pylon by turbulent wake structure, produces a change in the sign of the lateral force and the overturning moment as both are directional in nature. It was added that the wind shields as well helped to reduce the rate of change of wind forces. Without the shielding near the tower, the lateral force and the yaw moment coefficients reach their maximum values, when the vehicle is centered behind the tower(pylon). As well T.Argentini and E.Ozkan[3], reported that the presence of the tower does not shield the vehicle completely, but unexpectedly increase the aerodynamic loads due to transient and unsteady behavior of fields on the vehicle.

Tian Zhang and Wei Guo[4] studied and reported the effects of wind barrier and windshields on the side force (lateral force) and the moments coefficients. It was observed that the side force coefficient and moment coefficient of the vehicle decreased with the increasing height of the wind barriers, while the drag force coefficient and moment coefficient of the bridge increased with the increasing height of wind barriers. Tian Zhang and Wei Guo[4] also reported that the drag force and moment coefficients of the bridge decreased gradually upon modelling the porosity rate on wind-shields and wind barriers. This in-turn increased the side forces on the vehicle with increased porosity rate.

From these crosswind studies, it has been made evident and clear that the tower or pylon, decks and windshields are responsible for turbulent wakes and unsteady aerodynamic loads on the vehicles that pass across them. This will be further extended and studied in this thesis in terms of aerodynamic influences on the vehicle(truck) from pylon, deck, without/absence of pylon and deck, windshields, windshields with porosity models and transient(unsteady) case with dynamic mesh to investigate the unsteady aerodynamic effects on the truck as it passes through the bridge wake. The steady cases are analyzed using $RANS$ approach and unsteady cases are studied using $URANS$ approach.

3
Methods

In this chapter, the methods and the techniques adopted to simulate the external aerodynamics around the truck moving on a bridge structure are presented and discussed.

The methodology of this study is described in two parts. In the first section, it is discussed about the steady state CFD modelling of external aerodynamics around the truck. The unsteady CFD method will be discussed in the second section, along with a moving mesh strategy, to simulate the movement of the truck from far away from the pylon wake on the right to far away of the pylon wake to the left i.e; motion of the vehicle across the bridge deck. This method is carried out to study the transient, crosswind induced aerodynamic effects on side force and yaw moments on the truck.

3.1 Steady State CFD Modelling

The steady state model solves the governing transport equation as explained in chapter 2 eqn.2.9. The flow-fields are solved with respect to spatial variations and not against the time. In this method, the stable solution is found through an iterative approach using a matrix solver. The converged solution of the steady state model represents the stabilized and converged value of aerodynamic forces and coefficients in regard to a specific truck position and prescribed wind yaw angle. For the convergence criteria in this study, the side force coefficient was monitored and accepted to be a converged case, if the variation from last 500 iterations were not more than 5 counts. The steady state results correspond to the physics in three-dimensional case and do not reveal any information on the flow-fields with change in time.

3.1.1 Geometry and Model Development

The Computer Aided Design(CAD) model of the truck was available for this study. But, the 3D CAD model of the bridge elements (pylon, deck and windshields) were developed using Catia V5 pre-processing design tool. The entire geometry for the study and for CFD investigations is divided into 3 parts, namely, truck, deck and pylon. Once the model was developed, it was then transferred to StarCCM+ for further processes like meshing and assigning boundary conditions. The different parts of the model which required special focus on mesh setting or specific boundary conditions for assigned regions, were marked and given an identity to separate them in StarCCM+. The surfaces of the deck were split up using split by patch command to assign different boundary conditions. Entire surface of the pylon is maintained as one single entity without split up. The truck is split up as tractor(cab), trailer and axles to assign respective boundary conditions and special mesh settings. Few parts of the truck which were non-essential to model and mesh,

were removed from the existing model. The computational domain was then established through subtract operation comprising all the dedicated parts needed for the study and was then assigned to regions to prescribe the boundary conditions. The figs 3.1, 3.2 and 3.3 represents the modelled components for aerodynamic investigations.

Figure 3.1: Deck.

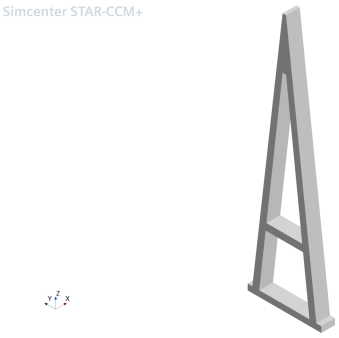

Figure 3.2: Pylon.

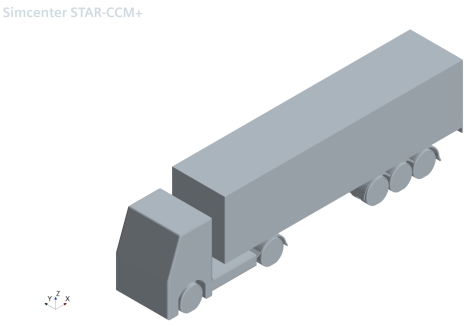

Figure 3.3: Truck.

3.1.2 Computational Domain

In CFD, the computational domain is the region of space where the numerical solutions are calculated. In an internal and external flows, the computational domain is defined by the confines of the geometry models and the volume inside the domain is discretized

into a computational grid. The properties of the flow-fields are calculated from the grid faces and stored in the respective nodes of computational mesh cells. This computational domain refers to a simplified form of the physical domain in terms of geometrical attributes and boundary conditions impositions and retains all the possible physically important interactions. The fig.3.4 shows the computation domain of this study with all the imposed boundary conditions. Similar kind of computational model was discussed by William.Y and Mohamed.E [5] in their work and investigated the crosswind aerodynamics for road Vehicles Using CFD techniques.

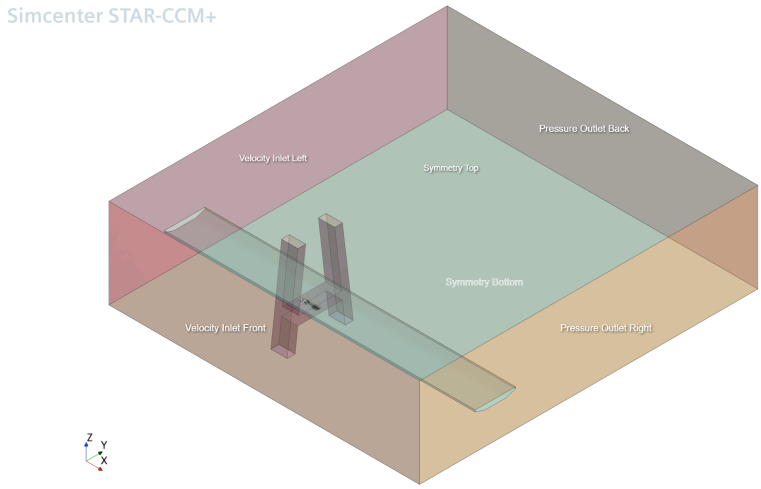

Figure 3.4: Computational Domain.

The domain in this case has two inlets and two outlets to take into the effect of crosswind inflow from the upstream directions to numerically solve and simulate the computational model at different yaw angles. The fig.3.5 represents the need for two inlets as the system will have two different velocity components due to side wind yaw angle.

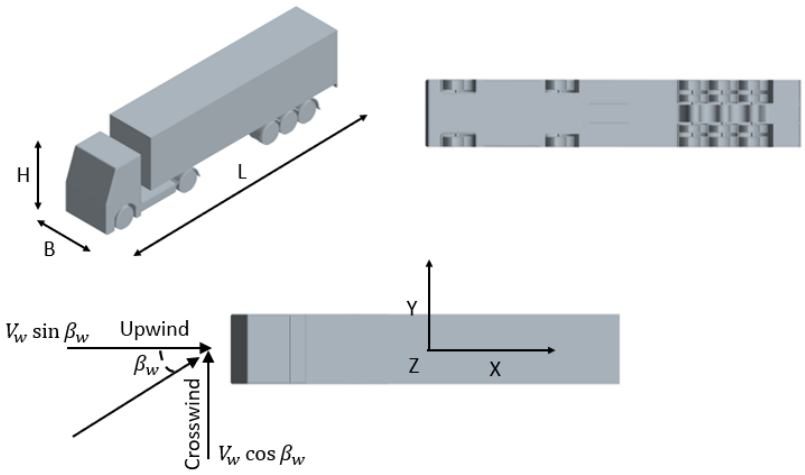

Figure 3.5: Crosswind Condition.

3.1.3 Geometry Surface Preparation

The surface repair tool in StarCCM+ was used to identify the error prone parts of the CAD, on its surfaces, feature edges and the pierced faces that are found with it. These issues are then fixed using the surface repair method and the geometry is then made prepared for the CFD investigations.

In-order to obtain a good mesh, a watertight and a non-intersecting geometry is necessary. Hence, the geometric faults such as gaps, intersecting and overlapping surfaces, needs to be fixed. These operations are performed using surface wrapper option. The Surface wrapper can be pictured as a sheet surface that is wrapped around the truck geometry and thus simplifies the geometry by covering all small gaps and as well removes the mismatches associated between the surfaces. In this method, wrapper with fine controls is used and the volume of interest is specified around the truck as the study is on external aerodynamics and then wrapped-in the areas where the fluid would be present, thus sealing the gaps. To further improve the quality of the volume mesh, surface remesher is as well triggered to retriangulate the surface cells and to have a better surface for volume mesh. The table 3.1 illustrates the settings adopted for surface wrapping of the truck.

Table 3.1: Surface Wrapper Controls

Feature description	Control Parameters
Base Size	0.05m
Target Surface Size	0.02m
Minimum Surface Size	0.005m
Surface Curvature	36.0
Gap closure	0.1m
Volume Of Interest	External

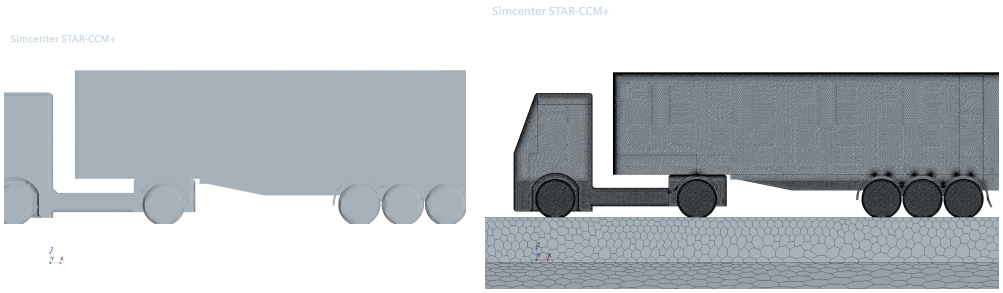

(a) Truck after surface wrap and surface repair

(b) Surface Remesher implementation on wrapped truck

Figure 3.6: Example of a surface wrapped truck and surface remesher execution

3.1.4 Computational Mesh Development

To solve the flow-fields, the geometry is split into smaller domains or cells which are of simple geometric shapes with nodes and faces. In these sub-domains, the governing equations are discretized and solved using $RANS$ approach. The computed values are stored in the respective cell nodes. The split-up of whole domain into small cells as control

volumes would give results with better accuracy, but it requires more computational power and resources to solve. This always needs a trade-off to decide the cells size in the different regions of volume of interest. Hence, the split-up into smaller cells is not uniform throughout the domain and instead the core areas or regions of interest are identified and provided with finer cells and rest of the domain is provided with relatively larger cells. This is done with a focus to keep the model, computationally efficient. It is always advisable to have as fewer cells as possible, but without any compromise on the stability of computed solution. So, the mesh development is a vital step to solve the flow physics within computational domain. The table 3.2 explains the meshing parameters employed for this case.

Table 3.2: Mesh Settings Employed for The Study

Feature description	**Control Parameters**
Base Size	3.6m
Target Surface Size	2.88m
Minimum Surface Size	0.144m
Surface Curvature	36.0
Number of Prism Layers on the Truck	6
Total Thickness of the Prism Layer	0.108m

3.1.5 Volume Mesh

The volume mesh is generated in the computational domain using Automated mesh in the solver. Polyhedral mesher along with prism layer mesher is chosen to mesh the whole volume. This uses an arbitrary polyhedral shaped cells to build the core mesh. Generally, for a three-dimensional case with random flow pattern, due to large turbulent wakes and strong re-circulation flows, the polyhedral mesher is preferred. The pseudo-random orientation of the cell faces, the mesh works better for the cases with flow direction that is random in different locations of the domain.

The prism layer cells are enabled near the wall region to ensure proper wall modelling and to have the wall $Y+$ within acceptable limits. The prism layer mesher generates the orthogonal cells in the closer proximity to the walls of the domain. This will resolve the gradients of the flow more accurately closer to the wall, as there will be a significant velocity gradient in the wall normal direction close to the vehicle surfaces. Walls are as well the source for vorticity, and therefore, prediction of flow around the walls are critical. Added to this, boundary layer formation over the wall surface is inevitable. The fig.3.7b, shows the achieved wall Y+ for the truck through the approached mesh controls. It can be seen that more than 85% of the truck is within the acceptable limits of wall Y+ as recommended by the Siemens Steveportal guide [6].

The surface remesher is also used as it re-meshes the initial surface to provide improvements on the quality of discretized mesh and makes it more suitable for the CFD flow simulations, thus, preventing the solution from divergence problems because of the mesh quality. It is used to retriangulate the surface based on the length of target edge and also omit specific surfaces or boundaries, thus preserving the original triangulation from the imported mesh. The surface remesher also ensures that all the triangles in the resultant

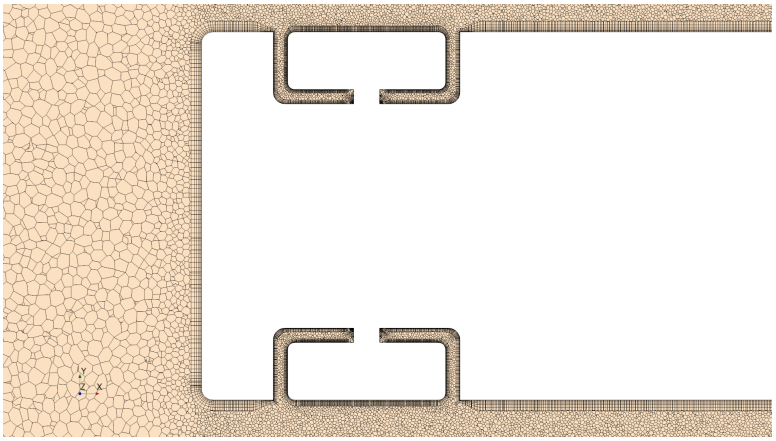

(a) Zoom-in View of Prism cells

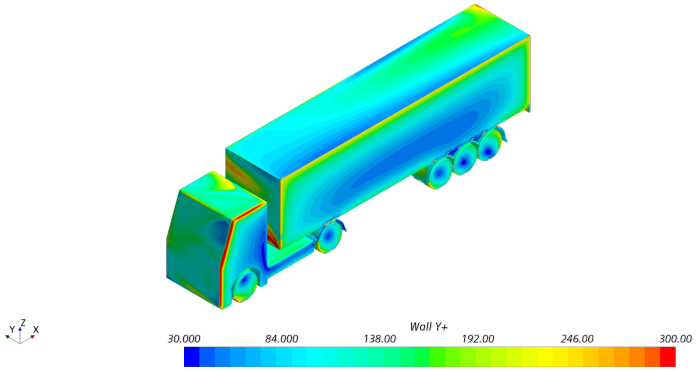

(b) Wall Y+

Figure 3.7: Prism cells zoom-in around tractor and Wall Y+ on truck

surface mesh have a quality greater than the specified value. This minimum quality is achieved by allowing the mesher to disregard feature edges, move feature vertices, and avoid projecting the vertices.

The fig.3.8 and fig.3.9 shows the volume mesh from top and front view for 30 yaw and 90 yaw crosswind conditions respectively. From the left figure, it can be seen that the refinements are progressively increased towards the right of the pylon. As for 30 yaw crosswind condition, the pylon deflects the flow and results in huge wake at an angle of 30 degree. Hence, to resolve the gradients effectively, the refinements are as well developed in such a way that the connecting diagonal points of all the refinement sections follows the 30 degree angle perspective with respect to wake flow direction. But for 90 yaw crosswind condition, the wake development around the pylon is relatively symmetric. Hence, the refinement sections were developed progressively in such a way that the turbulent wake structures will be captured, and the gradients will be resolved effectively on both sides of the pylon wake. Hence, unlike 30 degree yaw case, for 90 yaw, the refined sections are expanded progressively on either side of the pylon. The fig.3.9 shows the volumetric mesh on a cut section plane, viewed at the mid of the tractor from front. The refinement sections on the vertical axis Z are maintained in such a way to capture the wake flows

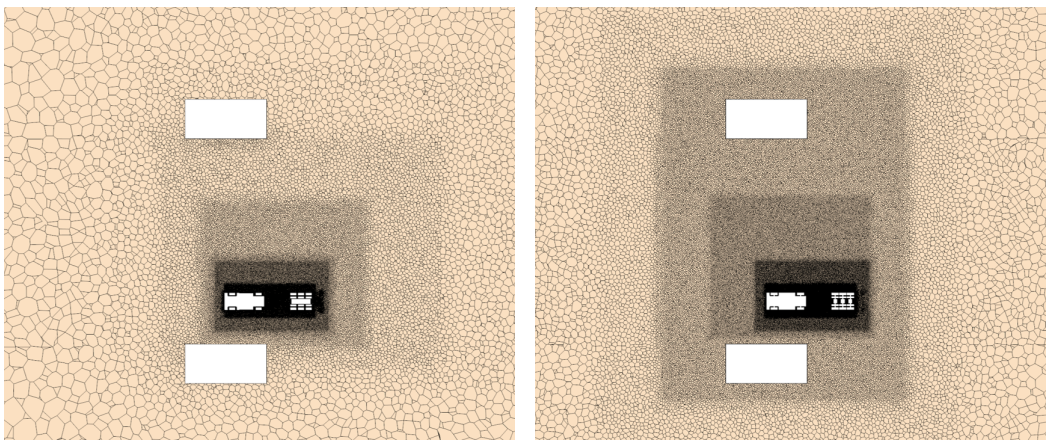

Figure 3.8: Top view of volume mesh for 30 yaw and 90 yaw

above the truck and to solve the gradients in the field effectively.

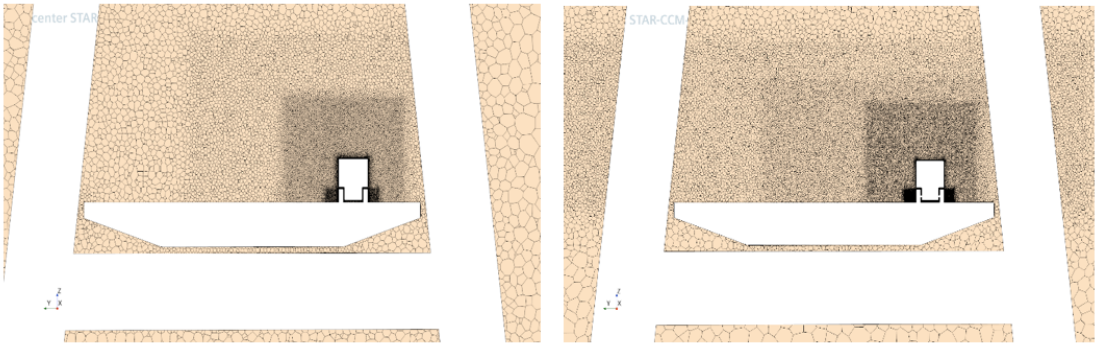

Figure 3.9: Front view of volume mesh for 30 yaw and 90 yaw

With this mesh configuration as mentioned in table 3.2, quite a stable solution was achieved. The monitored convergence criteria for the solution are the force coefficients, in particular, the side force coefficient is tracked as this study is based on crosswind aerodynamics. For both the 30 and 90 yaw side wind conditions, it was observed that the force coefficient showed insignificant fluctuations i.e; lesser than 5 counts in the last 500 iterations for a finely converged case.

From the fig.3.10 and fig.3.11, it is evident that the implemented mesh settings were fine enough to solve the flow fields, as it shows a good convergence in both residuals as well as the force coefficients. So, this mesh settings was then implemented for all the steady state modelling CFD simulations, to study the crosswind influence at different positions of truck on the deck on either side of the pylon. For all the cases, the side force coefficient (C_s) was monitored as the convergence criteria to stop the simulation.

3.1.6 Solver Physics

In order to simulate the fluid motion, it is necessary to choose models which collectively represent the analyzing case. In this section, the reasons for selecting a particular model and the type of solver and solver settings used for the CFD simulation to analyze this

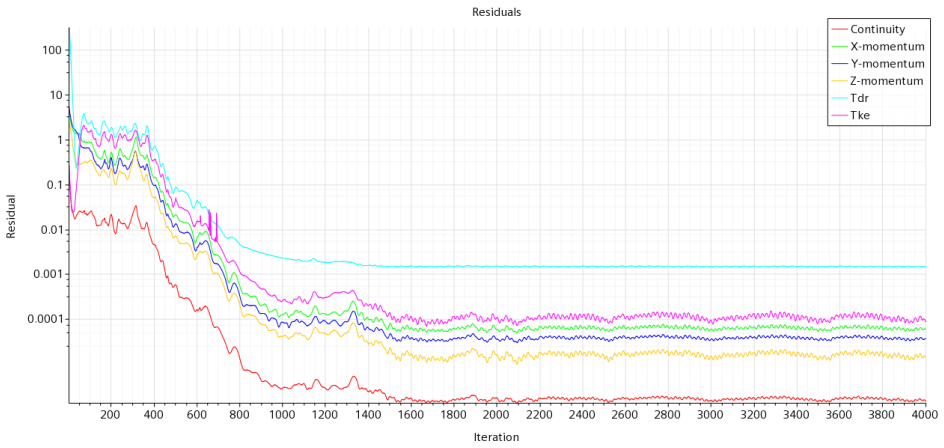

(a) Residuals 30 yaw

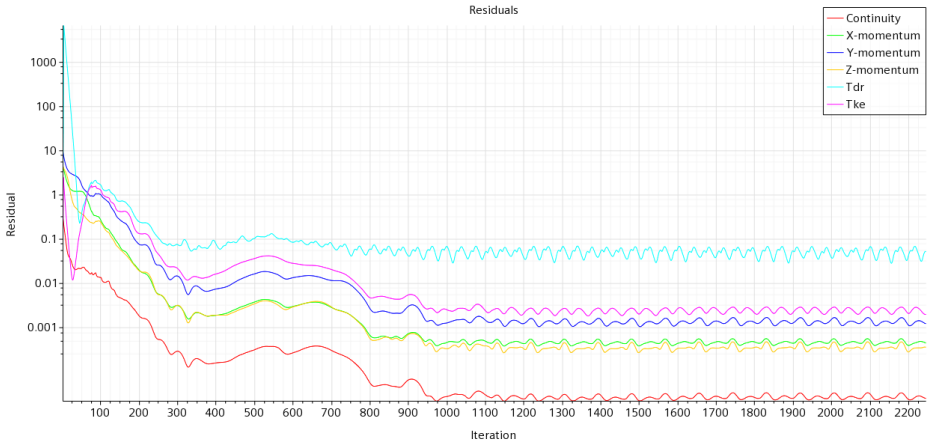

(b) Residuals 90 yaw

Figure 3.10: Residuals for 30 and 90 yaw wind case - Steady state modelling

case is presented.

The Navier Stokes(NS) transport equations are solved in three-dimensional space. In the steady state, the properties of the fluid considered are that of air at standard atmospheric conditions. Since, this case deals with low speeds and low mach, there will not be any significant change in the density. Hence, the constant density model (incompressible flows) is chosen as the equation of state to solve for the fields at constant density value.

The $k-\epsilon$ turbulence model is chosen for the study, as the area of interest is far away from the wall region and with a focus to analyze the far-field turbulent wakes. Within $k-\epsilon$ model, realizable $k-\epsilon$ turbulence model is selected to predict the turbulent scales. This option limits the shoot in viscosity ratio in the domain by scaling down the normal stresses, thus helps in providing a stable solution. In addition to this, two layer all $y+$ wall treatment option is chosen to effectively resolve the gradients closer to the wall, and as well to have a strong wall modelling in the simulation. The table 3.3 presents the chosen model and physics as a recommended settings for the analysis of crosswind aerodynamics for this particular case.

(a) Force coefficients 30 yaw

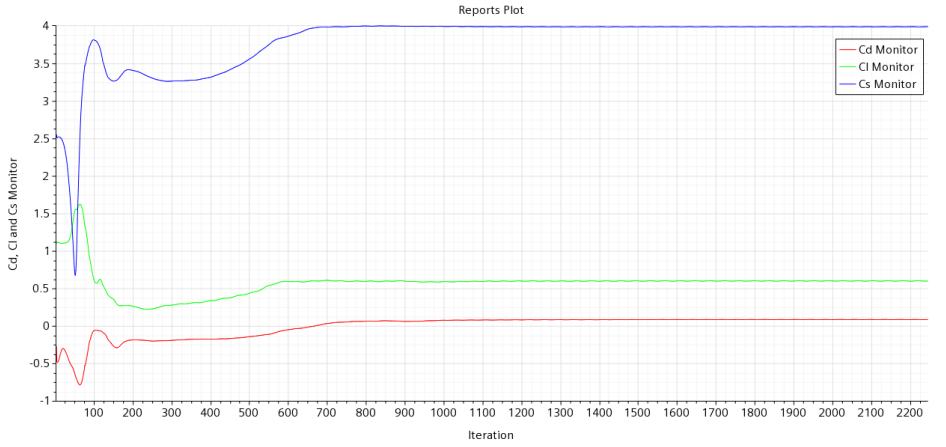

(b) Force coefficients 90 yaw

Figure 3.11: Force coefficients for 30 and 90 yaw wind case - Steady state modelling

Table 3.3: Solver Physics and Selected Models

Model group	**Preferred Model**
Space	Three-dimensional
Fluid	Air
Flow	Coupled Flow and Gradients
Equation of the state	Constant Density
State	Steady State Model
Viscous Regime	Turbulent and Reynolds Averaged Navier Stokes($RANS$)
Turbulence Model	Realizable $k-\epsilon$ Two Layer and All y+ Wall treatment(Wall function)
Optional Model	Cell Quality Remediation
Initialization	Grid Sequencing

The selected Coupled Flow model solves the conservation equations for mass and momentum equations simultaneously using a time-marching approach. Generally, for a steady state simulation, a pseudo-transient term replaces the physical time derivative in the

transport equations. The solution in each cell nodes is iterated independently with an optimal pseudo-time step computed locally with respect to Courant-Friedrichs-Levy(CFL) number specified. In the solver, it is as well possible to choose a user defined CFL number. The advantage with coupled solver is that the solution can be accelerated by using high CFL number with proper computational mesh to obtain convergence within fewer iterations. With the coupled Solver, the expert initialization, grid sequencing(GS) is triggered. This performs, the normal initialization on a series of coarser meshes followed by the computation of an approximate inviscid solution in the flow domain. This is carried out through a series of iterations that are run with the coarsest mesh and eventually compute an approximate solution for the current mesh. This option prevents the need to initialize the flow-field parameter in the domain as an input trigger. The Grid Sequencing (GS) as well ensures faster and more robust convergence of the flow solution in the computational domain.

3.1.7 Boundary Conditions

The Boundary conditions (BC) are essential constraints that are needed to solve a boundary value problem. These conditions are employed to model the case in a closer way to reality. Upon initialization of BC at a particular boundary, the flow-field values that are varying across the domain and away from the boundaries will be in close concurrence with the initialized conditions and modelled physics. As well, the varying fields in the domain, will eventually be satisfied at the specified boundary.

Table 3.4: Boundary Conditions

Regions	**Boundary Conditions**
Tractor of truck	Wall and No-slip
Trailer of truck	Wall and No-slip
Wheels	Rotational
Deck	Wall and No-slip
Pylon	Wall and No-slip

The fig 3.12 illustrates the i component of velocity on truck and wheels. Since, wall boundary condition is specified on the truck, it shows zero velocity on it. The wheels are given tangential velocity specification with respect to local coordinate systems and the rotation is prescribed about j, with the rotational rate corresponding to $25m/s$. Hence, the velocity j(y-component) on wheels is observed as zero, as the velocity exists in only i component. As well, it can also be seen that, bottom of the wheels have $25m/s$ while at the top, the wheels show -$25m/s$. This is due to the fact that, the velocity is a vector quantity which has a directional property, hence the change in sign is observed with magnitude being the same.

The fig.3.13a illustrates that, the velocity component i is insignificant in the front of the truck. But, rear to the truck, a small acceleration of flow and gradients of velocity field i can be seen. This is due to the fact that, the upstream velocity component j from y-direction is been redirected to i i.e; x-direction, due to the presence of sharp bluff bodies like pylon and trailer of the truck. But the velocity component i is almost insignificant except from these areas, as this is not the main source of inlet i.e; not the velocity inlet boundary.

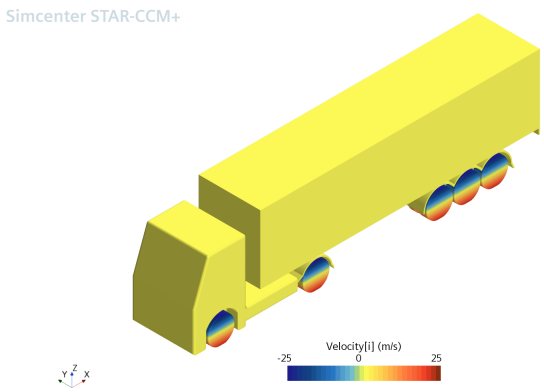

(a) Velocity component i

Figure 3.12: Velocity component i on the truck

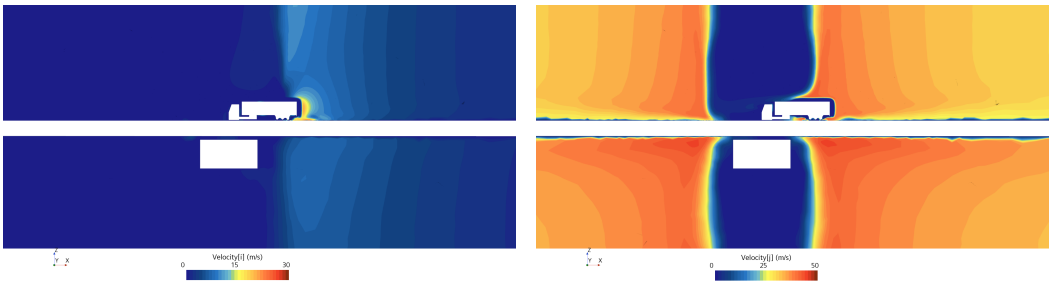

(a) Velocity i in the Domain

(b) Velocity j in the Domain

Figure 3.13: Velocity in i and j component in the domain in the crosswind downstream view

The fig.3.13b illustrates that, the velocity component j is the only main significant component in the domain. This is due to crosswind domain setup conditions. The j component is along the y-direction, which is the crosswind upstream direction, prescribed as velocity inlet boundary. Due to the presence of pylon, the velocity j in the middle of the domain is almost negligible as there is a flow separation and formation of wake. The acceleration of the flow is thus around the wake flow structures, hence, the velocity is maximum. It can also be seen that the velocity j on the deck is negligible i.e, zero, in both the cases due to wall boundary condition.

The fig.3.14 depicts the top view (resultant magnitude) for the fig.3.13a and 3.13b. Hence, the figs.3.12, 3.13 and 3.14 illustrate that all the prescribed boundary conditions in the domain are fulfilled successfully.

3.2 Unsteady CFD Modelling

In this section, the moving mesh concept is adopted to simulate the movement of truck across the deck and pylon to perform the transient study. Unsteady simulations for different yaw wind conditions are carried out and the crosswind aerodynamics on the

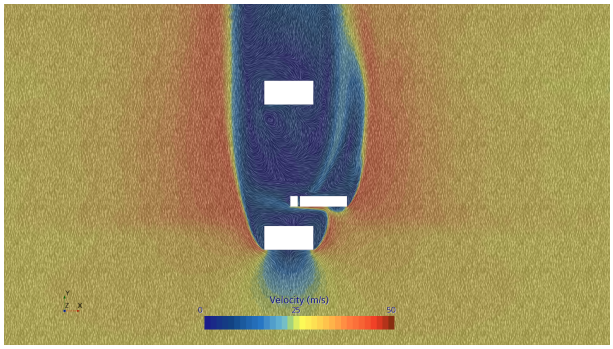

Figure 3.14: Velocity corresponding top view

truck is analyzed and quantified in terms of side force and yaw moments. The motion of the truck and time dependency-based flow-field computation is vital to mimic the real-time scenario.

3.2.1 Solver Physics - Unsteady

The physics models that are chosen for the steady state are the same followed in the unsteady model as well. The main change that is made in the solver setup is switching the time domain from steady to implicit unsteady. In implicit unsteady method, solution is calculated by both the current state of the system and the immediate-next state of the system with respect to successive time steps. The immediate-next state of the system is an unknown and it is computed iteratively and hence it is defined as implicit unsteady. The time step chosen for the study is derived from the requirement on the overset mesh methodology and the demand on flow-field data requirement. It is necessary for the overset mesh, when in motion and in a given time step, to not move more than one single neighboring cell. The requirement for this study is that, the motion of the truck is to be started far away from the pylon wake on the right (from top-view) and should be translated to far away off the pylon wake to the left (from top-view). This covers 150m of truck motion across the deck with the truck velocity at $25m/s$. These are the two main conditions to decide upon the total physical time of 7.5s with the time step of 0.003s and 5 inner iterations for the study. The steady-state solution is used for the initialization of the unsteady models.

Table 3.5: Solver Physics and Selected Models - Unsteady

Model group	Preferred Model
Space	Three-dimensional
Fluid	Air
Flow	Coupled Flow and Gradients
Equation of the state	Constant Density
State	Implicit Unsteady
Viscous Regime	Turbulent and Unsteady Reynolds Averaged Navier Stokes($URANS$)
Turbulence Model	Realizable $k-\epsilon$ Two Layer and All y+ Wall treatment(Wall function)
Optional Model	Cell Quality Remediation
Overset Model	Overset Conservation (Auto recommended option)

3.2.2 Computational Mesh

The motion of the truck is obtained by using overset mesh strategy. This is also known as Chimera method in which one or more dynamic meshes are patched to a static background mesh. The moving mesh and the stationary mesh exchange flow field information through the interface established between the two meshes. The process of interface creation follows a two-step approach. In the first step, active, inactive and acceptor cells are determined. The Cells that are at the boundary of each mesh (both dynamic and static part) are considered as the active cells. The cells that are setup next to these active cells are known as acceptor cells. These acceptor cells are to be surrounded by the donor cells. The exchange of flow-field information from the background to overset mesh through the interface is featured and contributed by the donor cells. In this study, a small separate block is created around the truck, called moving overset. This box encapsulates the whole truck to enable the movement across the domain. The overset region (small box around the truck) and the background region are meshed separately to develop as a two separate regions. The overset volume around the truck is set as an overset boundary. The existing background mesh and the overset mesh overlaps with each other upon creation of interface. In few cases, a zero-gap interface is to be used when there is no gap between the parts inside the overset mesh and the background mesh. For this study, zero gap interface is not required to be implemented. It is as well important to have same geometrical attributes of mesh across the interface of both regions as recommended by StarCCM+ user guide[6].

3.2.3 Boundary Condition Specifications

All the boundary conditions that are given for the steady-state case are same for transient case as well. The difference is that, in this case, there are two regions, one for background static part and other for moving overset part. The dynamic overset block is given the overset boundary condition with motion translation setting as per the model requirement.

The fig.3.16 illustrates the overset boundary around the truck, which will have the translation motion across the domain, to capture the flow-fields at different locations and at

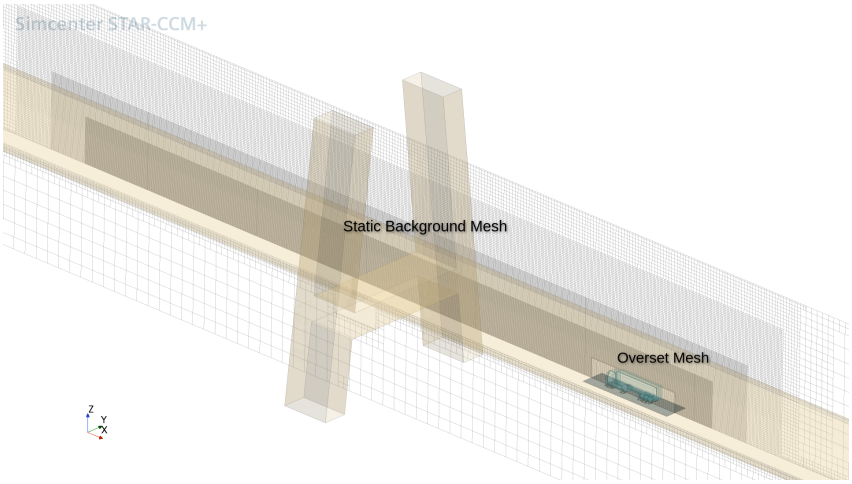

Figure 3.15: Representation of Overset and Background Static Mesh

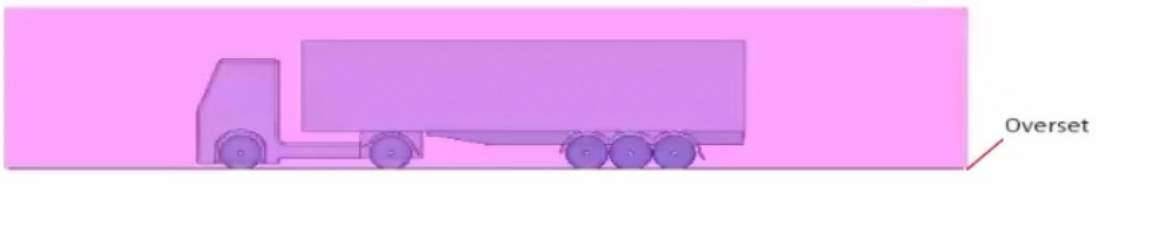

Figure 3.16: Representation of overset region around the truck

different positions of the truck.

With these implications in the unsteady solver, the CFD simulation is run for a physical time of $7.5s$ with a time step of $0.003s$.

4
Results and Discussion

In this chapter, the results from steady state and unsteady/transient CFD simulations for different cases on crosswind aerodynamics are presented and discussed.

4.1 Steady state simulations

The steady state simulations are performed to investigate the effects of different bridge structures in the aerodynamic forces and moments on the truck. The influence from the bridge structures viz., deck, pylon and windshields are presented. The CFD simulations are performed for the truck at different positions across the bridge deck and the computed generalized C_s trend is discussed in detail. As well, the arguments on the effects from windshields as a solid part and with porosity models are expressed in the final section of steady state simulations. 30yaw and 90yaw are the side wind conditions that are chosen for all steady state simulations.

4.1.1 Baseline model and study on the influence of different bridge structures

The position chosen for the baseline model and to study the influence of bridge structures like pylon and deck in terms of both combined effect and as well on an individual basis is represented in the fig.4.1. This position is preferred for the sake of having similarity in comparison metrics between different bridge structures, as the influence from all different elements of bridge is highly effective at this position. A shift from this position to either side will not have the presence of pylon and as well as the turbulent wake.

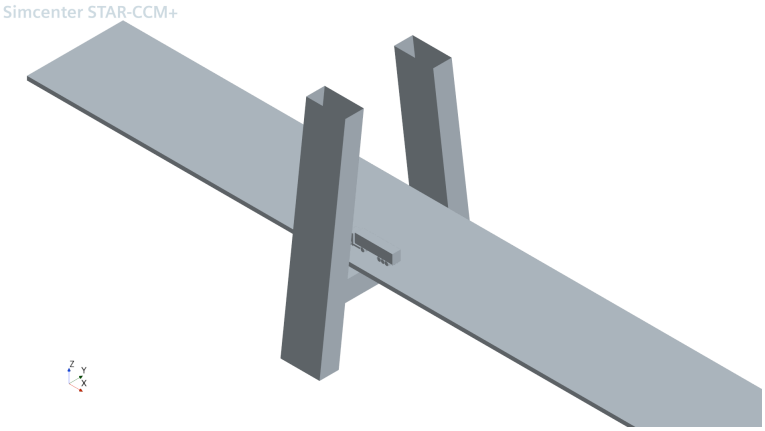

Figure 4.1: Respective position of truck in the domain

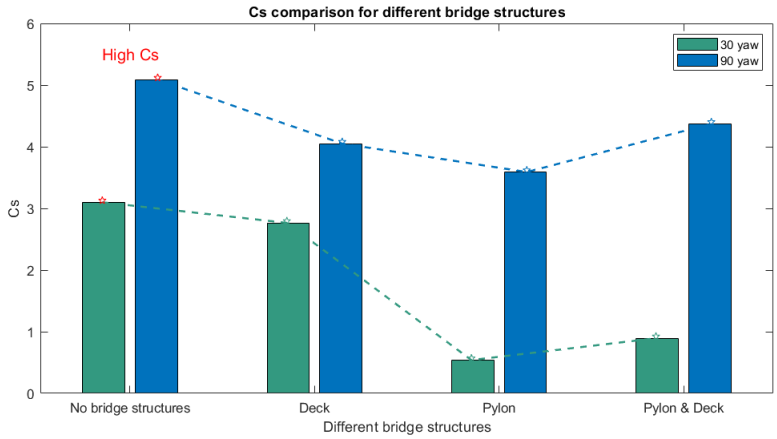

Figure 4.2: Influence of different bridge components in the side force on truck

The fig.4.2 illustrates the resultant side force on the truck due to the presence of different bridge structures.

The computed values of side force coefficients correspond to the position of the truck represented in the fig.4.1. This position is taken and considered to be the baseline of this study to develop further models as explained earlier. As this is close to the pylon, that creates a large wake flow in the domain. The truck in this position is partially shielded by the pylon and partially exposed to the incoming side wind. This, as well, provide information on how big the flow separation is when the separated flow(wake) from the pylon is further separated from the trailing edge of the trailer upon incidence.

From the fig.4.2, it can be seen that the presence of pylon acts as a shield. The incoming side wind will have flow separation from the pylon and results in large wake structures. The truck at this position is not completely exposed to side-winds, and thus reduction in side-force coefficient C_s is observed. On the other hand, in the absence of bridge structures, the truck is completely exposed to side winds as there is no shield to divert the flow. Hence, in this case, the truck will experience more side force, as shown in the fig.4.2.

As well the presence of deck alone, reduces the side force on the truck by 21.5%. The reason is that, the incoming side wind upon interaction with the deck, is separated and a localized wake is developed beside the lower half of the truck as shown in the figs.4.3a and b. So, only the upper half of the vehicle is exposed to the strong side wind. It is due to this reason, the presence of deck reduces the side force on the truck.

The figs.4.4 a and b represent the top view, with crosswind aerodynamics influenced by the presence of deck alone. It is evident that the wake generated by the deck alone is very less significant when compared to the wake from the pylon as shown in fig.4.5 a and b for 30 yaw and 90 yaw. Thus, the side force on the truck is high in the absence of pylon, as the vehicle is only partially shielded by flow separation from deck. It can be seen that the pylon completely shields the truck from harsh side winds at this position.

A small region of acceleration, that is seen in the fig.4.4, which is on the other side (opposite to the side of wind incidence) of the truck is due to acceleration of the flow in

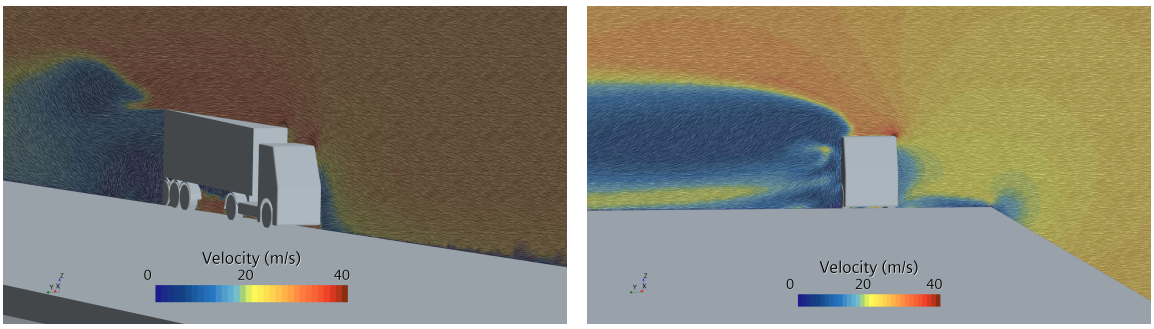

(a) 30 yaw **(b)** 90 yaw

Figure 4.3: Influence of deck on 30 yaw and 90 yaw side wind conditions

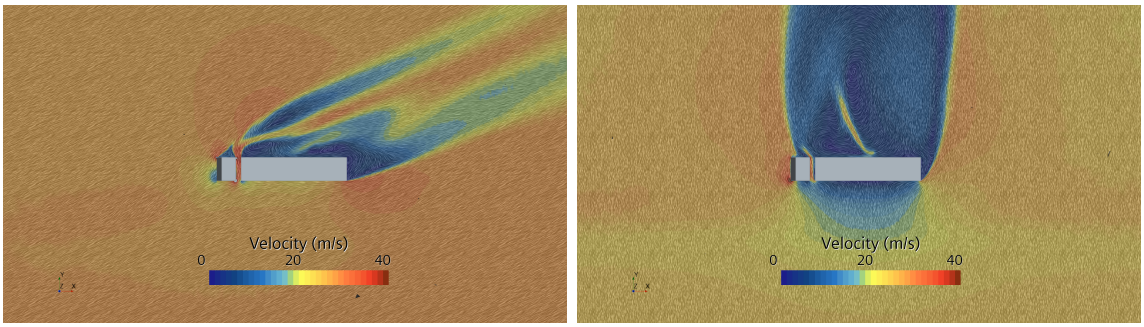

(a) 30 yaw - only deck - top view **(b)** 90 yaw - only deck - top view

Figure 4.4: Influence of deck on 30 yaw and 90 yaw side wind conditions - Top View

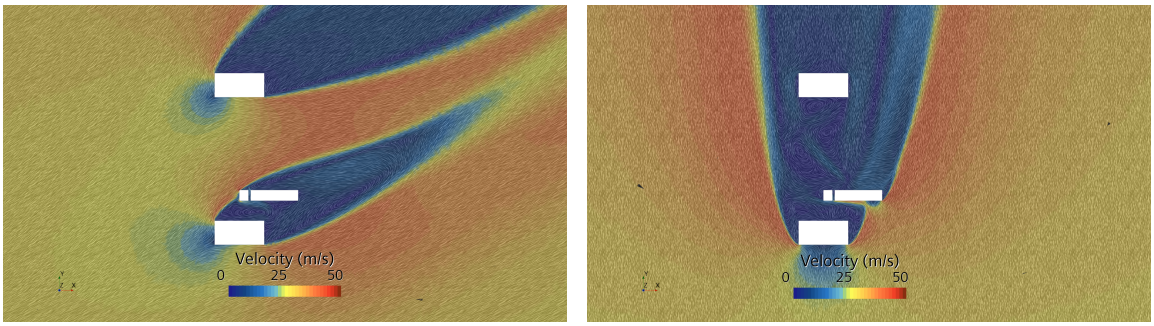

(a) 30 yaw - only pylon - top view **(b)** 90 yaw - only pylon - top view

Figure 4.5: Influence of pylon on 30 yaw and 90 yaw side wind conditions - Top View

the gap under the truck, between wheels and as well between truck and trailer. This is show in the figs.4.6 a and b.

The fig.4.7 represents the front view of velocity field but without the influence of any bridge structures like pylon, deck and windshield. When compared with fig.4.3b, it can be seen that there is a strong velocity gradient near the exposed side of truck. This indicates a strong stagnation of incoming wind at the truck side surface as there is no shields and any wake flow due to flow separation from the bluff bodies like pylon and deck. Thus, the absence of shielding from the deck and pylon, makes the vehicle more

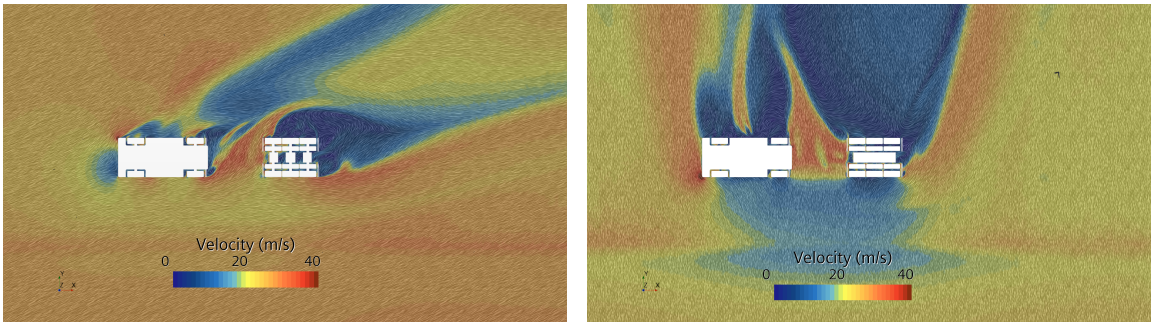

(a) 30 yaw - wheel cut view - top **(b)** 90 yaw - wheel cut view - top

Figure 4.6: Cut section at the middle of wheels for 30 and 90 yaw - Top View

exposed to incoming side winds and results in increased side force as shown in fig.4.2b.

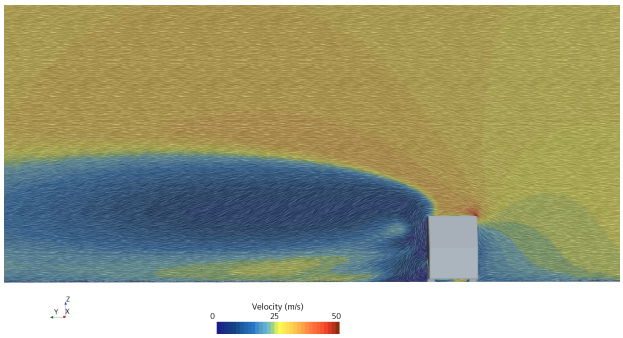

Figure 4.7: No influence from bridge structures

The pressure coefficients on truck are shown in the fig.4.8. The figs.4.8a and 4.8b represents the influence from deck and pylon on an individual basis. This illustrates that there is larger stagnation area of fluid at front in the absence of pylon. Thus, the truck is susceptible to more side force in the regions that are away from the pylon.

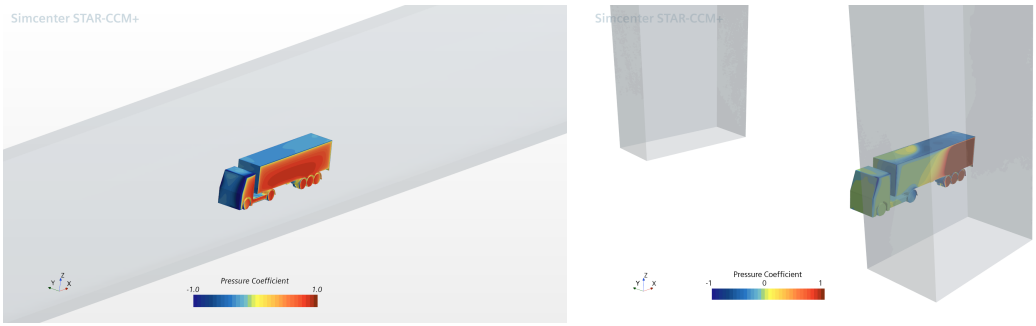

(a) Pressure coefficient - Presence of Deck **(b)** Pressure coefficient - Presence of Pylon

Figure 4.8: Pressure coefficient comparison

4.1.2 Investigation of side force on truck at different positions of the bridge

In this section, investigations carried out with steady state CFD models for different positions of truck on the bridge with the bridge structures like pylon and deck are presented.

The fig.4.9 depicts the trend obtained for side force coefficient C_s on the truck, that is computed at various positions across the deck with pylon. This is performed for two side wind cases, i.e, 30 yaw and 90 yaw. Both the side wind cases show similar trend but with one obvious reason that the C_s on truck and the side forces from 90 yaw is on a higher scale when compared against 30 yaw.

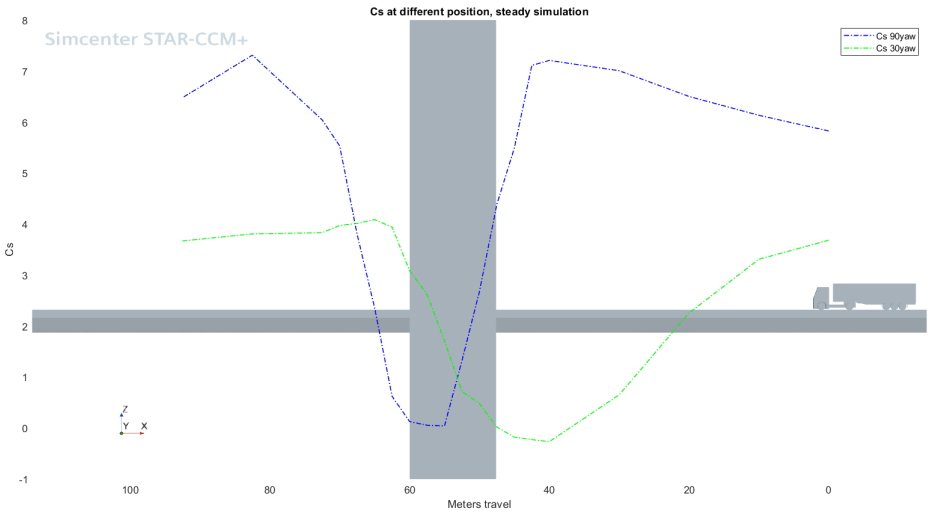

Figure 4.9: C_s at different positions of truck on bridge - Steady State

The fig.4.9 illustrates the side force coefficients(C_s) for 30 yaw and 90 yaw at different positions, as the vehicle travels on the bridge (from right to left) as represented. As discussed earlier, it is interesting to note that the truck will have minimum side force when it approaches the intense wake region. Depending on the side wind yaw angle, the position of minimum C_s changes. The wake from 90 yaw side wind is closely symmetric about the pylon and hence the minimum C_s appears close to the center of pylon. For the 30 yaw side wind, the separation of incoming side wind has 30 degree deflection, i.e, 30 degree about the axis of deck. The position of turbulent wake shifts from the center of pylon. Thus, the minimum C_s is shifted accordingly, which is yaw angle dependent.

In the immediate vicinity after the wake, there is a huge acceleration of the flow which results in maximum side force on the truck. This is due to the fact that the aerodynamic loads increase with respect to flow velocity. So, the maximum side force coefficient C_s, can be seen in this region for both 90 yaw and 30 yaw case. After the maximum point, the C_s on the truck drops with a steep slope which indicates the strong velocity gradient that is present due to turbulent wake. It is as well interesting to note that the slope of the C_s trend formed with respect to the minimum C_s is symmetric. This indicates that the vehicle is moving into the wake from free-stream and accelerated flow (right side); and as well the vehicle is coming out from the wake and enters the free-stream again (left side). Far off the wake on both right and left, the C_s is almost constant as the incoming

wind velocity is almost at free-stream range with negligible velocity gradients. It is this position, where the turbulent wake structures of the pylon no longer have influence.

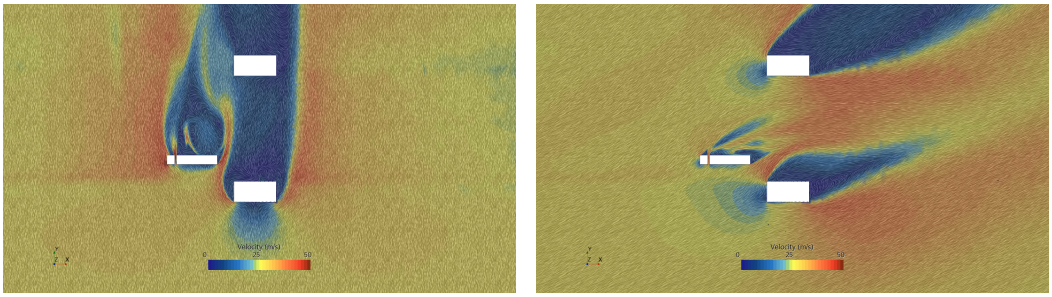

(a) 90 yaw case **(b)** 30 yaw case

Figure 4.10: Flow separation from the truck - for different yaw conditions

From the fig.4.9, it can be observed that, for the yaw wind at 30 degree, the side force on the truck is minimum when compared against the yaw wind at 90 degree. This is due to the fact that at 30 yaw, the side wind is at an angle of 30 degree with respect to the direction of motion of the truck. The incoming wind is deflected by the edge of trailer upon incidence and results in separation as shown in the fig.4.10b. So, the exposed side surface of the truck for 30 yaw side-wind is minimal when compared to 90 yaw. In case of 90 yaw side-wind, the wind directly hits the side surface of the truck in an axis perpendicular to the direction of vehicle motion as shown in the fig.4.10a. This results in more stagnation on the side surface as it is completely exposed, and thus increases the static pressure. Due to this fact, an increased pressure coefficient and C_s is observed for 90 yaw side-wind scenario.

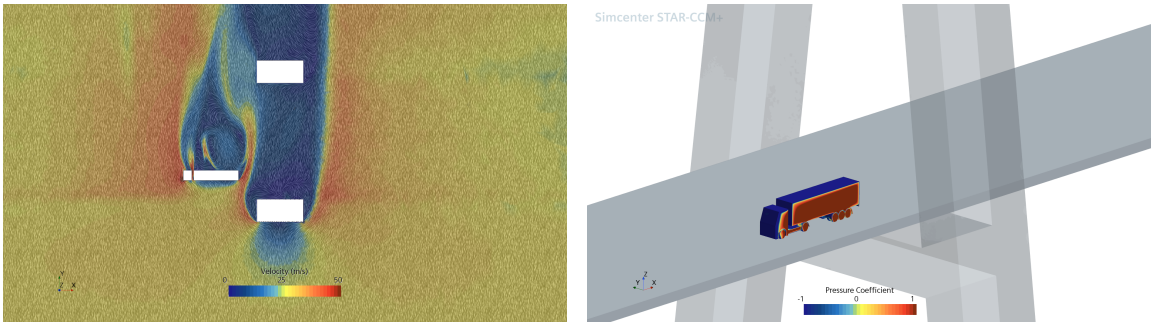

(a) Velocity - Top view **(b)** Pressure coefficient

Figure 4.11: Velocity and pressure coefficient at a position immediate left to the pylon wake - 90 yaw

The figs.4.11 and 4.12 represent the position of the truck, immediate next (at left) to pylon wake. The velocity and the pressure coefficient in these figures correspond to 90 yaw and 30 yaw side wind conditions respectively. This is the position, where the C_s tend to increase with a steep slope as in fig.4.9, once the vehicle travels and comes out of the turbulent wake region. And the vehicle in this position is no more shielded by pylon and completely exposed to the strong side winds.

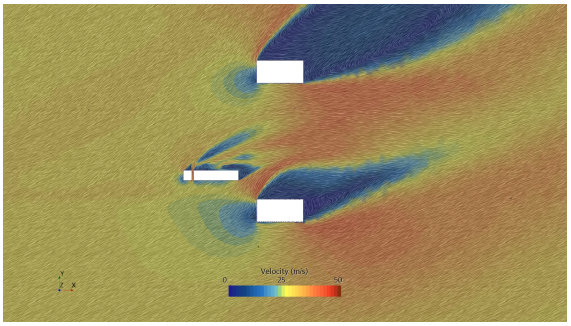

(a) Velocity - Top view

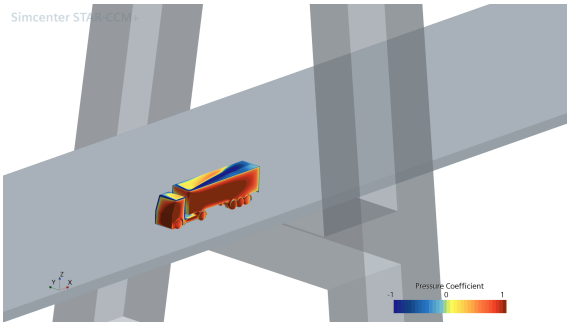

(b) Pressure coefficient

Figure 4.12: Velocity and pressure coefficient at a position immediate left to the pylon wake - 30 yaw

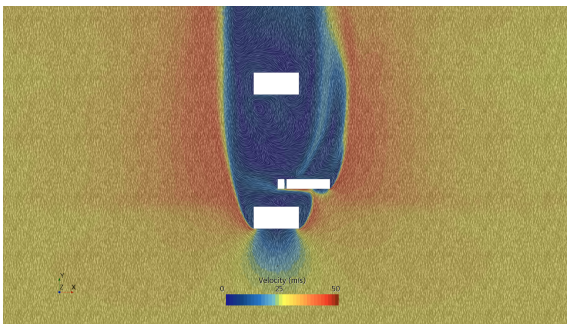

(a) Velocity - Top view

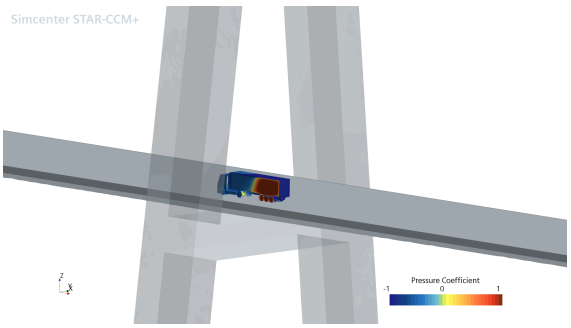

(b) Pressure coefficient

Figure 4.13: Velocity and pressure coefficient at a position close immediate to the pylon wake - 90 yaw

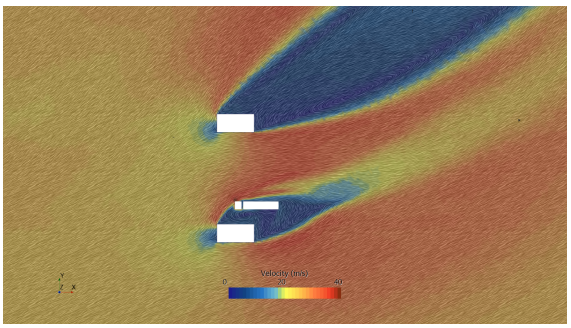

(a) Velocity - Top view

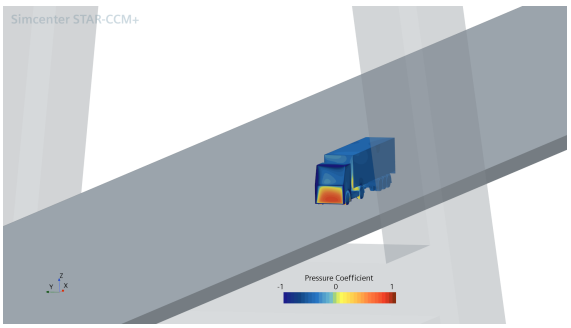

(b) Pressure coefficient

Figure 4.14: Velocity and pressure coefficient at a position close immediate to the pylon wake - 30 yaw

The figs.4.13 and 4.14 illustrate the position of truck in the wake region for 90 yaw and 30 yaw side wind scenarios. This is the position, where the C_s is found to be minimum in the trend shown in fig.4.9 and hence the low side force on the truck. The huge wake is the effect from the presence of pylon as illustrated in fig.4.5.

The fig.4.15 represents the position of the truck on the right, far off from the pylon wake.

This is the region, where the truck is completely exposed to side winds. There is neither any shields from pylon nor any influence from the gradients of strong wake. As the vehicle further move towards the left from this position, the C_s tend to gradually increase due to the interaction with accelerated flows around the pylon wake as shown in the fig.4.9. This is illustrated for 90 yaw side wind condition.

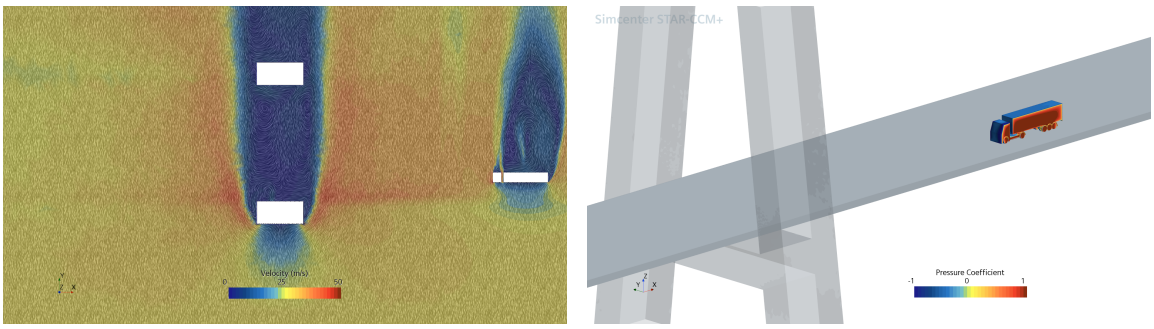

(a) Velocity - Top view **(b)** Pressure coefficient

Figure 4.15: Velocity and pressure coefficient at a position far off from the pylon wake - 90 yaw

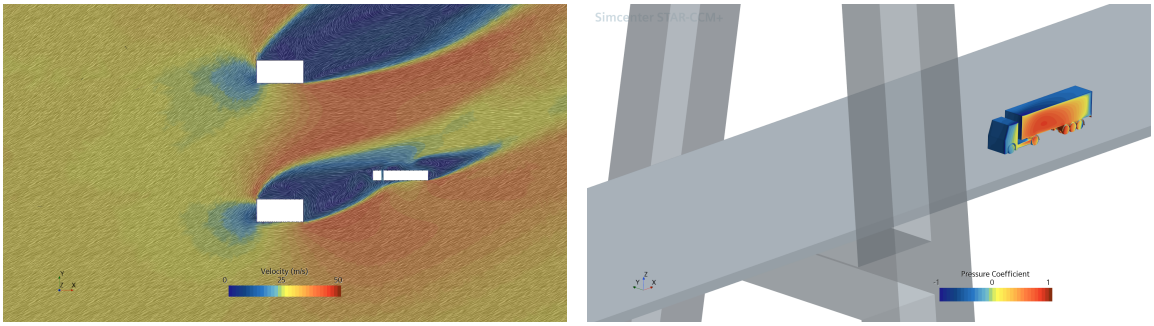

(a) Velocity - Top view **(b)** Pressure coefficient

Figure 4.16: Velocity and pressure coefficient at a position far off from the pylon wake - 30 yaw

But at 30 yaw side wind condition, the trend of C_s tend to decrease as the truck approaches to the wake region (in the left) from far off position in the right. Reason behind this is, the fact that the 30 yaw side wind is at an angle of 30 degree with respect to the vehicle motion, the wake is extended far away from the pylon. Thus, the movement of the truck when comes closer to/into this region, the trend shows reduced C_s, and thus minimum side force. This condition is illustrated in the fig.4.16 which corresponds to the trend behavior shown in the fig.4.9.

Fig.4.17 represents the wind induced yaw moments on the truck at different positions from 30 yaw and 90 yaw side wind scenarios. It is observed that the yaw moments on the truck are fairly constant in the regions far off from the pylon wake, on either side. The increase in the yaw moment is observed as the vehicle approaches the wake region. This is due to the varying pressure distribution on the truck surface as shown in fig.4.16b, that

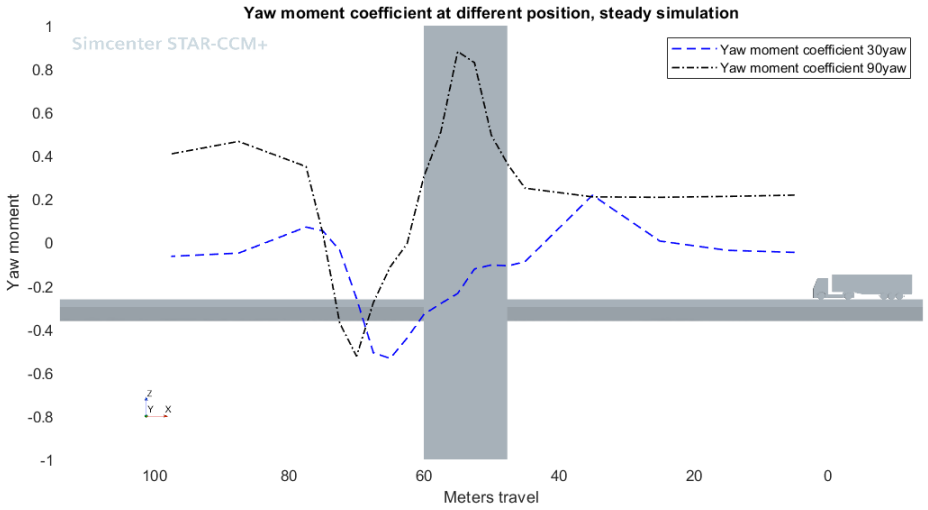

Figure 4.17: Yaw moment at different positions of truck on the bridge - Steady State

arises from the presence of gradients in the field because of the influence of turbulent wake and flow separation from huge bluff body. To the left side of the scene in the fig.4.17, negative values can be seen which is due the fact that, moments are direction in nature and depends on the pressure distribution on truck. Minimum yaw moment on the truck is seen, when the vehicle is completely in the wake region, where the pressure coefficient C_p is very minimum and insignificant.

4.1.3 Study on windshield influence and porosity modelling

Windshields on bridge deck plays an important role in shielding the vehicles from harsh side winds. The incoming flow upon incidence on windshields, gets separated and diverted. A localized wake region is developed due to this separation and is observed beside the wind incident surface of truck. So, only a portion of exposed side (a portion of projected area) of the truck will be hit by the crosswind, and thus reduces the side force acting on it. In this study, the effect from different heights of windshields and its influence on the aerodynamic forces on truck is presented. The fig.4.18 depicts the presence of windshield on the bridge deck.

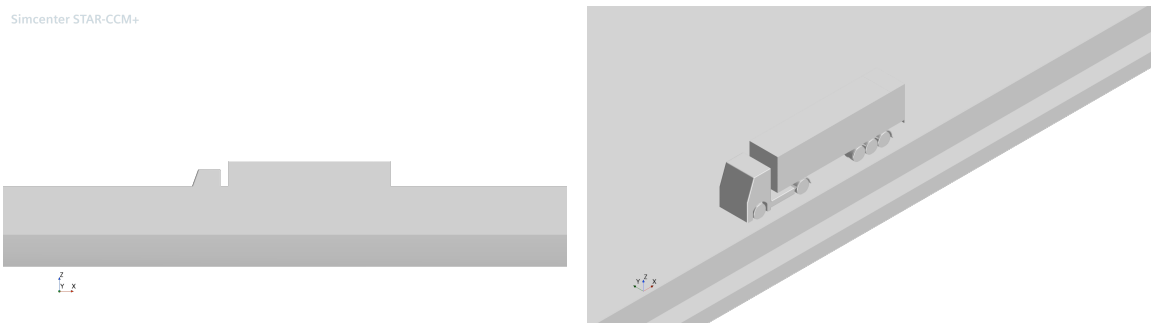

(a) Model with windshield - Side view

(b) Model with windshield - Perspective view

Figure 4.18: Windshield on the deck

The fig.4.19 represents the flow diversion (side wind flow) from the windshield upon incidence. This safeguards the truck from being exposed to high side winds, and thus minimize the intensity of side force acting on it. A portion of wake flow is generated in the space between wind shield and the truck. As well, above the edge of trailer in the wind incidence side, a huge acceleration of the flow is observed.

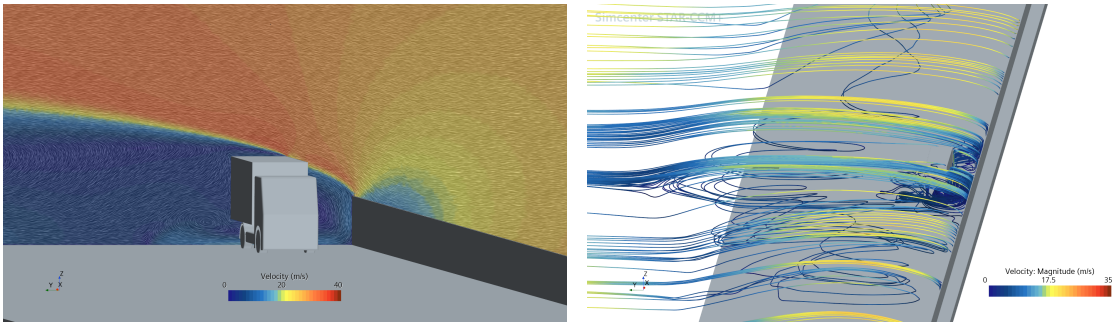

(a) Velocity scene **(b)** Streamlines

Figure 4.19: Influence of windshield

The above fig.4.19 illustrates the effect of solid windshield without any cutouts. But the bridge structure constructors develop windshields with cutouts to ensure structural integrity and weight optimization parameters. So, the windshields with cutouts will play an additional role in this case apart from shielding the truck through flow separation and diversion. There is a huge acceleration of air flow through the cutouts, and this does not shield the truck from the side winds. In this case, an increase in C_s is observed when compared to the windshields with no cutouts.

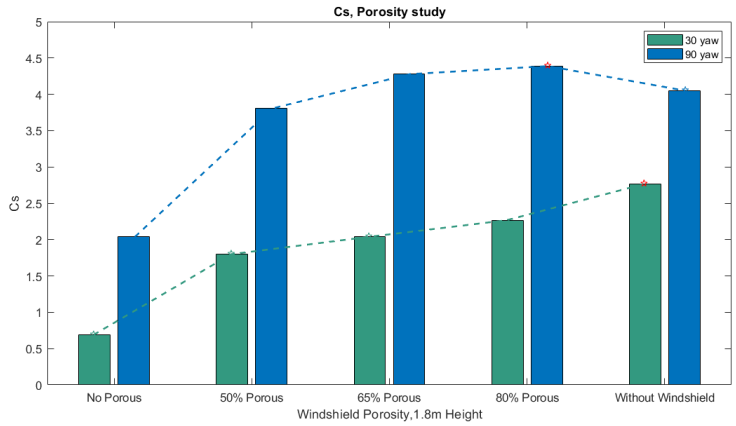

Figure 4.20: C_s Comparison for windshields with different porous area based on 1.8m height

The fig.4.20 shows the fact that, more the cutout in windshields, more the C_s and side force on the truck. For 30 yaw, it shows a progressive increase with increase in cutouts in the windshield. The maximum C_s on the truck is absorbed for the model without windshield as there is a complete exposure of projected area. On the other hand, it is interesting to note that, for 90 yaw the C_s shows a decreased value for the case with no windshields when compared against the windshields with 50% and 80% cutout. This is

due to the fact that, the windshield with more open cutouts accelerates the air flow to the surface of the truck for 90 yaw side wind case. This results in an increased stagnation pressure on truck from the incoming flow with more kinetic energy and results in an increased pressure coefficient C_p on truck. For 30 yaw case, even with the acceleration of wind through cutouts, the incident flow is again diverted with a separation from the truck - trailer gap and from the trailer trailing edge as the angle of incidence is at 30 degree. This flow deflection does not happen with 90 yaw side wind scenario.

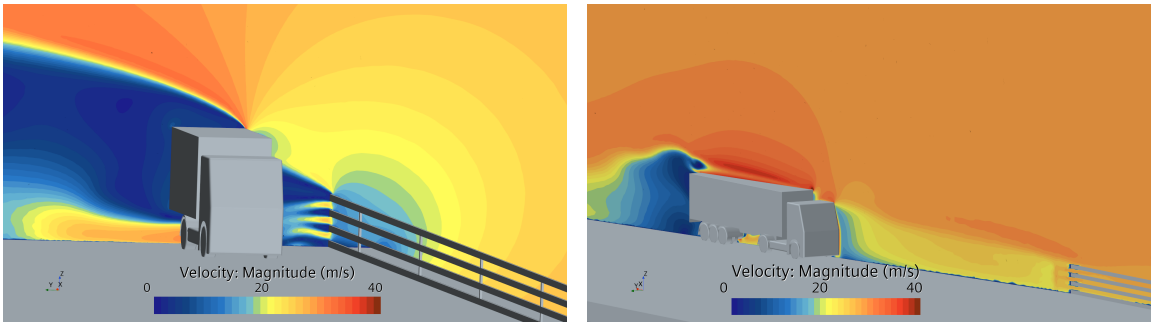

(a) Velocity scene - 90 yaw **(b)** Velocity scene - 30 yaw

Figure 4.21: Influence of windshield cutouts - 50% cutout

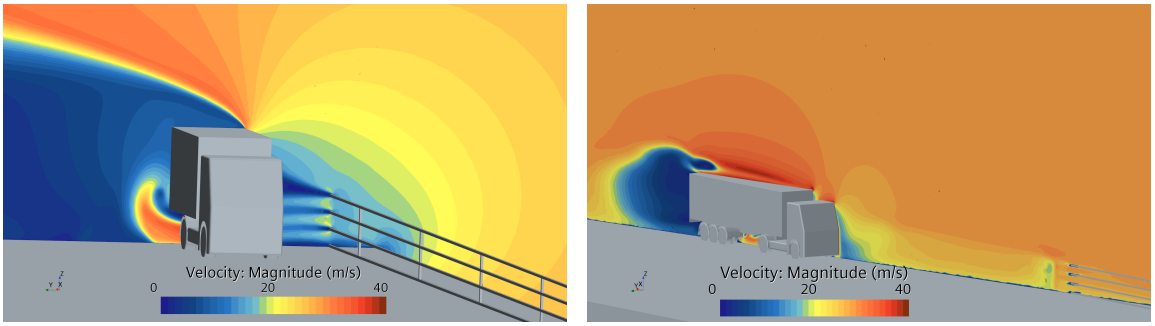

(a) Velocity scene - 90 yaw **(b)** Velocity scene - 30 yaw

Figure 4.22: Influence of windshield cutouts - 80% cutout

The fig.4.21 illustrates the acceleration of flow through the porous provided in the windshield. Since in 90 yaw case, the direction of side wind is perpendicular to the vehicle motion, the accelerated flow with high kinetic energy through the cutouts directly hits the vehicle surface and results in strong stagnation. Thus, this increases the pressure coefficient C_p and the side force on truck. But for 30 yaw case of side wind, the accelerated flow that pass through the cutouts is again deflected by the leading edge of trailer, resulting in separation and static pressure loss. Thus, the 30 yaw case shows decreased C_s and the side force. This deflection of flow by the trailer for 30 yaw case is illustrated by the fig.4.21b. On comparing the fig.4.21 and fig.4.22, it can be understood that more the cutout, more is the acceleration of the flow through it. Hence, higher values of C_s and side force on the truck is seen.

The fig.4.23 and fig.4.24 show the pressure coefficient on the truck for 30 and 90 yaw side wind conditions and correspond to 50% and 80% cutout on windshields. It is evident

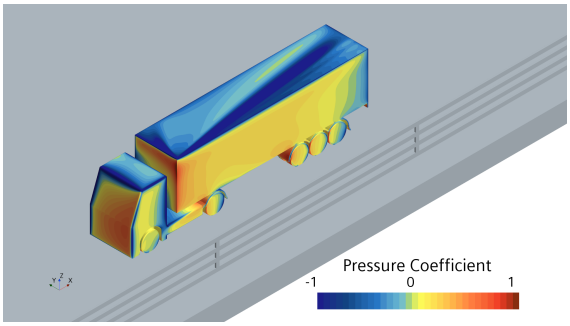

(a) Pressure coefficient - 50 percent cutout on windshield

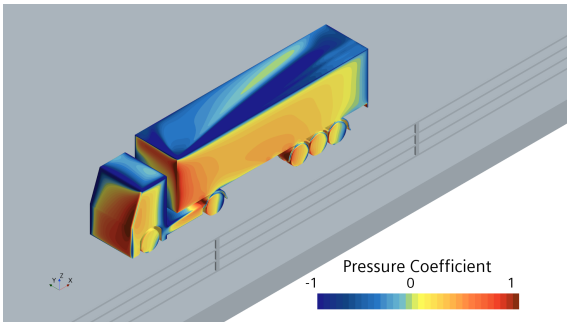

(b) Pressure coefficient - 80 percent cutout on windshield

Figure 4.23: Pressure coefficient - 30 yaw - For 50 and 80 percent cutout on windshield

from both the figures that, higher the cutout then higher is the C_p on the truck. For 30 yaw case represented in fig.4.23 a and b, a significant gradient can be observed near the trailing edge of trailer, which indicates the flow separation and pressure loss region that incurred upon the incidence of 30 yaw side wind. Also, it is interesting to note the presence of gradients on the top of trailer for 30 yaw case.

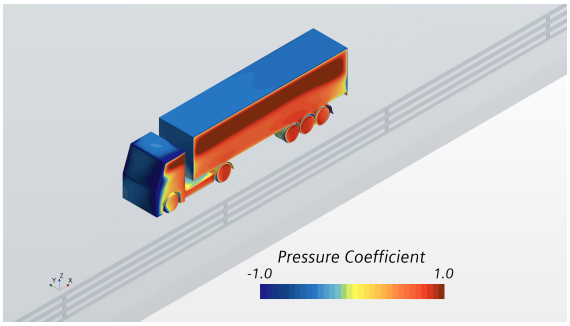

(a) Pressure coefficient - 50 percent cutout on windshield

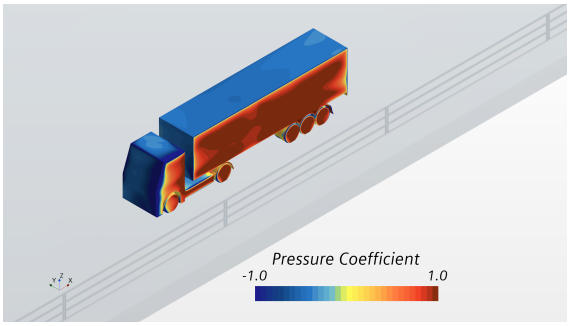

(b) Pressure coefficient - 80 percent cutout on windshield

Figure 4.24: Pressure coefficient - 90 yaw - For 50 and 80% cutout on windshield

From the fig.4.25, it can be seen that the pressure coefficient (C_p) is found to be higher for the case with 80% porous windshield when compared against the scenario of no windshield. This is observed for 90 yaw side wind condition. This is due the fact that, the presence of 80% porous windshield results in more stagnation, in the region of wind incidence and as well close to the side surface of the truck. Upon interaction of the two stagnation regions, the static pressure on the truck increases, and thus resulting in higher side force (C_s). In case of no-shields, there occurs only one stagnation region beside the truck side surface and hence the side force acting on the truck is comparatively lesser.

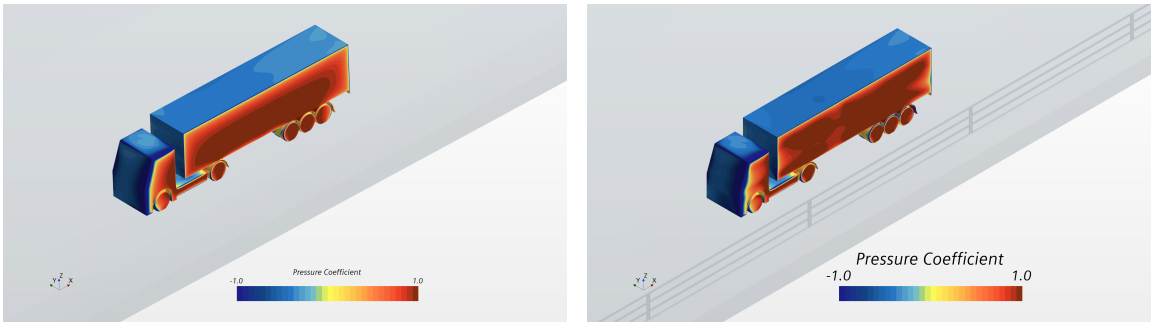

(a) Pressure coefficient - No windshield **(b)** Pressure coefficient - 80% cutouts

Figure 4.25: Comparison of pressure coefficient between no windshield and 80% porous windshield

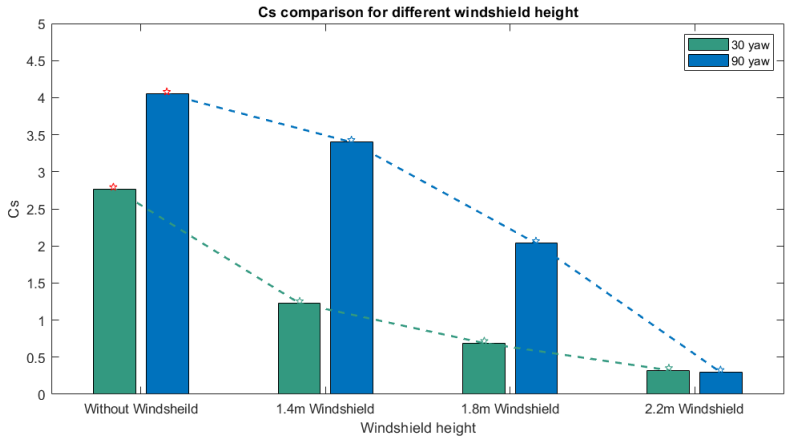

Figure 4.26: C_s Comparison for different heights of windshield

The presence of solid barriers reduces the aerodynamic loads on the vehicles. As well, the reduction of wind induced aerodynamic loads is directly related to the height of the barriers. The fig.4.26 illustrates the reduction in C_s with increase in the windshield height. As it is seen in the fig.4.19 that the windshields divert the incident flow to top of the truck and hence the vehicle's amount of exposure to side winds is dependent on height of the windshield and as well on the wind incidence angle. Higher the windshield, lesser is the exposure of truck and hence minimum is the side force and C_s. Also, Chen and Ning [7], and, Xiang.H and Li.C [8] investigated the effects of solid wind-barriers(windshields) and claimed that, the presence of shields, minimize the aerodynamic loads on vehicles driven on bridges.

4.2 Unsteady simulations

The solutions computed simulation is used to initialize the unsteady simulation. As discussed in the Chapter3, the overset mesh methodology is adopted to translate the truck across the bridge. The total physical time for this unsteady case is chosen with respect to truck's translation velocity (as in real-case scenario) and the desired travel distance. The time step and the number of inner iterations are kept in such a way to

achieve a good CFL and convergence for the case. The unsteady simulations are carried out for 30 ,60 and 90 yaw side wind conditions. The results from the 60 yaw side wind unsteady case will be presented in this section. Wang and Bin [9], also used $U - RANS$ method but with SST $k - \omega$ turbulence model and investigated the aerodynamic force coefficients on moving vehicles on bridge deck. The obtained side force coefficient from Wang and Bin [9] is in close accordance with the present study.

4.2.1 Production and dissipation of turbulent wake structures at different positions across the bridge

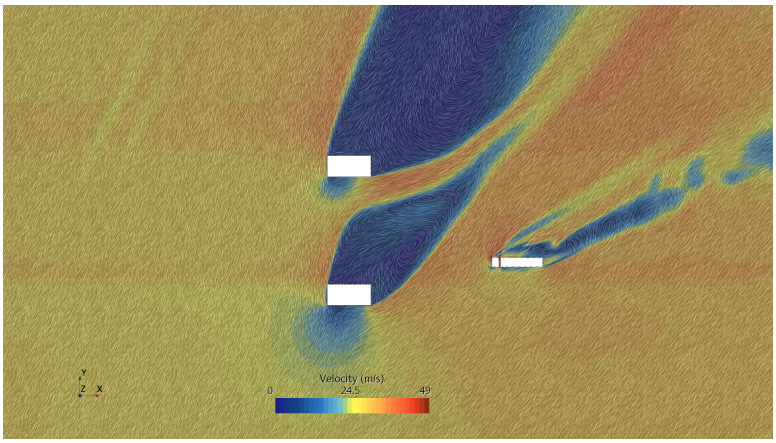

Figure 4.27: Velocity scene for 60 yaw - Truck position at 1.785s

The fig.4.27 illustrates the position of truck after a travel time of 1.785s. It can be seen that, the truck in this position is about to enter the accelerated flow region, that is next to the 60 yaw wake of pylon. It is also observed that a part of wake from the truck trailer seems to dissipate, and this results in shredding of large vortex structures.

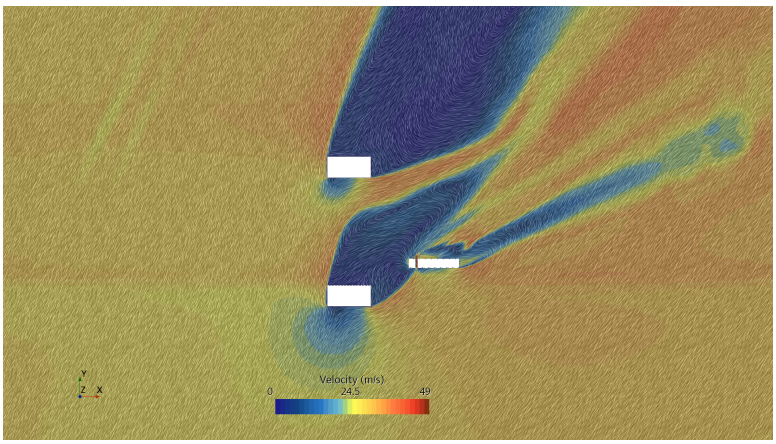

Figure 4.28: Velocity scene for 60 yaw - Truck position at 2.940s

The fig.4.28 shows that the truck enters the wake of pylon. As it passes through the accelerated flow piercing the pylon wake at front, the wake structure from the truck gets intensified. This is the result of interaction of turbulent structures with a moving bluff body(truck).

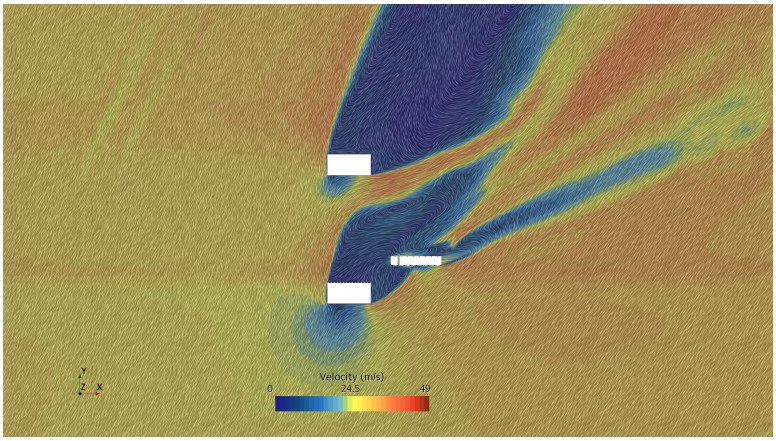

Figure 4.29: Velocity scene for 60 yaw - Truck position at 3.186s

The fig.4.29 corresponds to the position, where three-fourth of the truck is in the wake flow. As the vehicle penetrates through this turbulent zone, resulting in vortex shear and the wake gets attached to the trailer body and eventually gets separated from the edge of the trailer in the direction according to the side wind yaw angle.

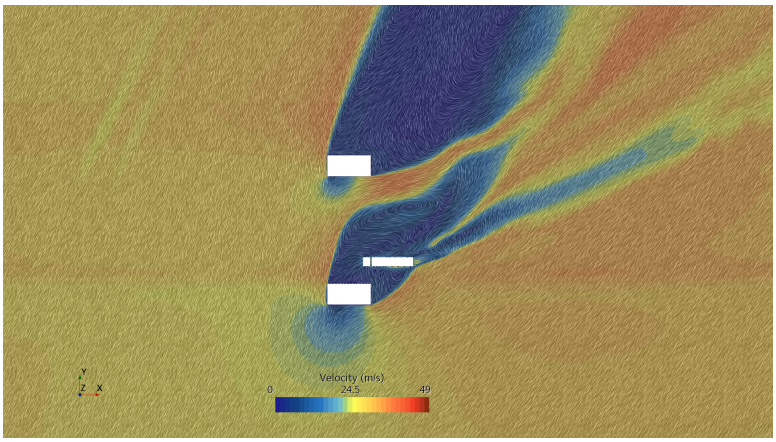

Figure 4.30: Velocity scene for 60 yaw - Truck position at 3.570s

The fig.4.30 shows that the truck is completely inside the vortex dominated turbulent wake region. Due to the interaction of the pylon wake with truck, a new wake structure is developed with regard to the flow separation from the trailing edge of trailer and remains attached to the pylon wake. This clearly shows that, a moving or a dynamic bluff body will have the influence on wake's strength.

The figs.4.30 and 4.31 depict that the truck is completely inside the wake of pylon. This is the position, where the vehicle is completely shielded from the side wind and has minimal side force and C_s. This can be seen in the fig.4.37.

The figs.4.32 and 4.33 show that the truck squeezes out the wake and comes out from the turbulent region of pylon. It can be seen that the wake of the truck tends to get separated from the trailer, interacts with the wake between pylon, and thus shows a strong re-circulation zone with large turbulent eddies. As the vehicle travels out of this region, a small portion of wake remains attached to the trailer that is in the opposite side of yaw

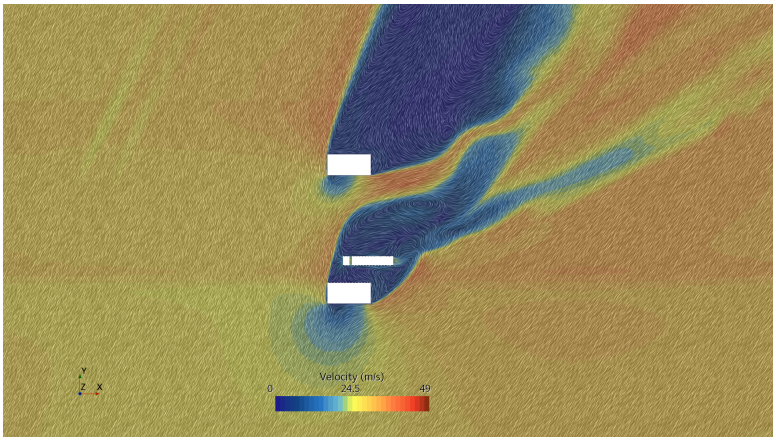

Figure 4.31: Velocity scene for 60 yaw - Truck position at 3.852s

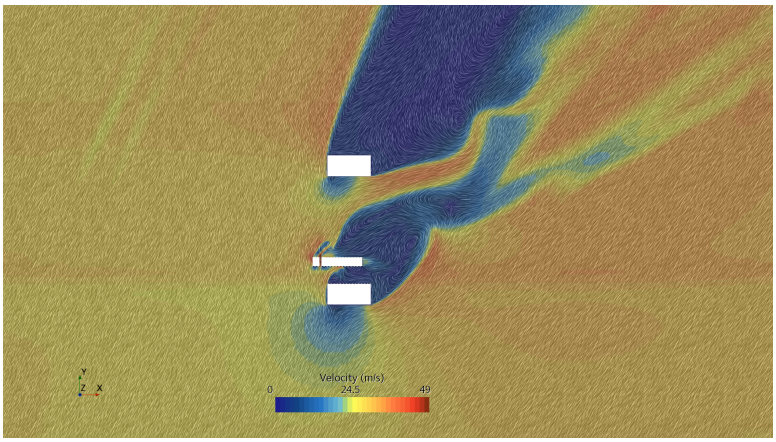

Figure 4.32: Velocity scene for 60 yaw - Truck position at 4.272s

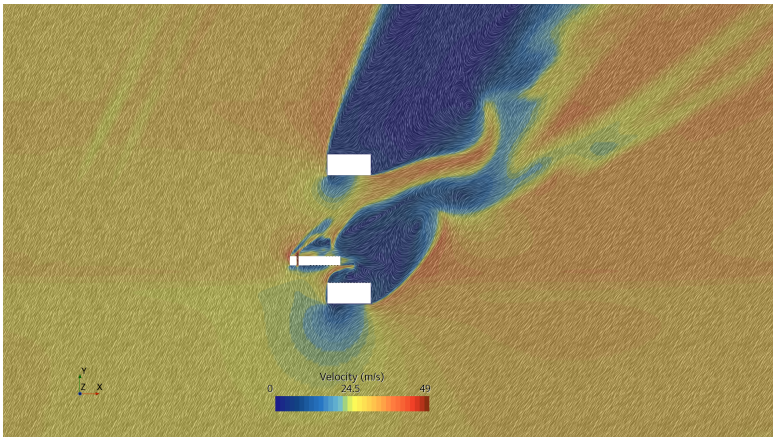

Figure 4.33: Velocity scene for 60 yaw - Truck position at 4.587s

wind incidence.

The figs.4.34 and 4.35 illustrate that the truck is completely out of the pylon wake. The wake from the truck trailer carries the pylon wake which later gets separated and dissipated. This is the region, where the side force on the truck starts to increase as the vehicle is completely exposed to side winds as shown in the fig.4.37.In all the stages, it

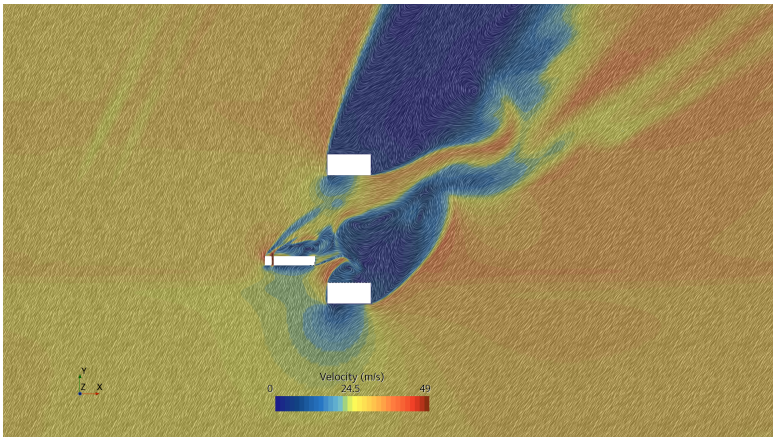

Figure 4.34: Velocity scene for 60 yaw - Truck position at 4.935s

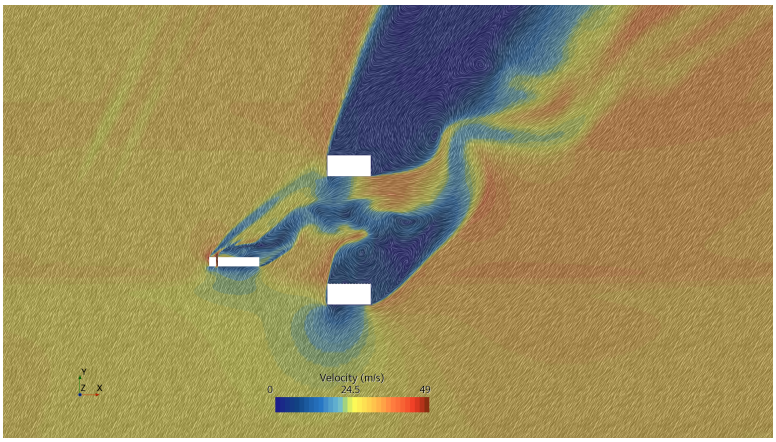

Figure 4.35: Velocity scene for 60 yaw - Truck position at 5.706s

can be seen that the production of turbulent wake structures declines over time i.e; it dissipates. This shows that the production equals the dissipation as per the law of energy spectra.

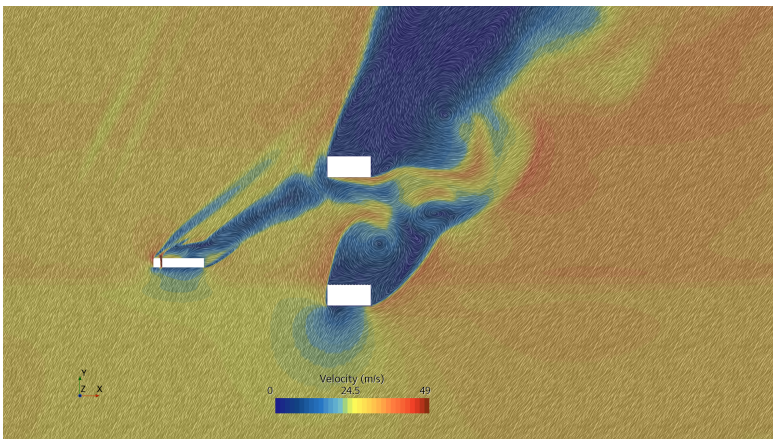

Figure 4.36: Velocity scene for 60 yaw - Truck position at 6.477s

4.2.2 Trends of C_s and yaw moment coefficient for different side wind yaw angles

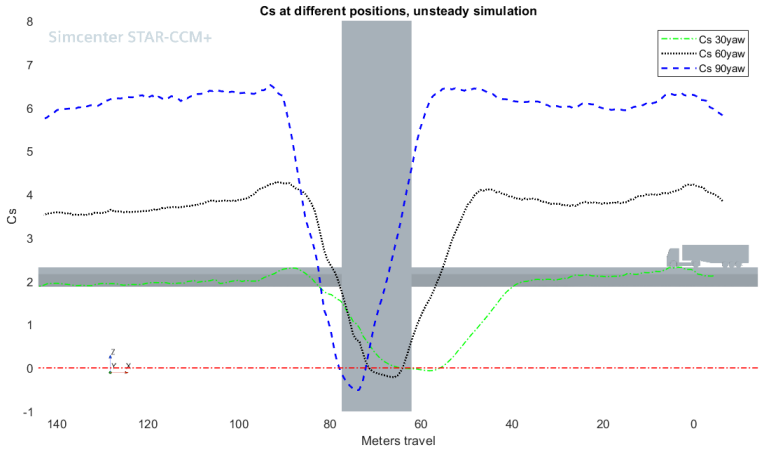

Figure 4.37: C_s at different positions of truck on the bridge - Unsteady case

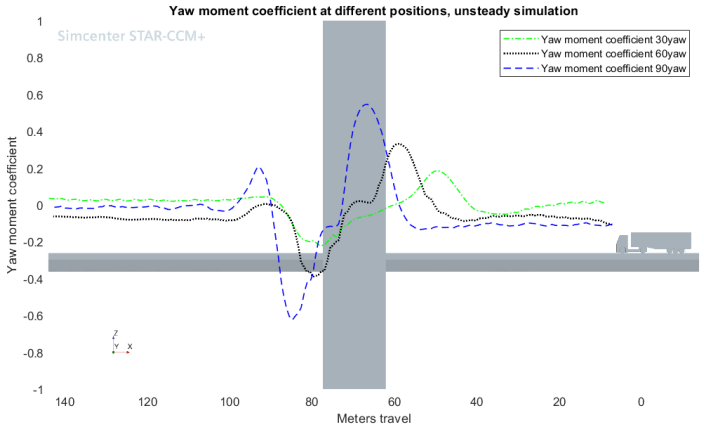

Figure 4.38: Yaw moment coefficient at different positions of truck on the bridge - Unsteady case

The figs.4.37 and 4.38 correspond to the side force coefficient C_s and yaw moments acting on the truck at different positions on the bridge, which is purely wind induced. The physics behind the trend obtained on C_s and yaw moments for this case is same as for the steady case simulations as discussed earlier. The negative values of yaw moments for the truck position at the left of pylon is due to the direction change, as the moment in clockwise direction is considered to be positive and negative for the anti-clockwise direction.

4.2.3 Comparison between steady and unsteady trends

The figs.4.39a and 4.39b show the comparison between the computed C_s values for steady state and unsteady(transient) case at different positions of truck on the bridge. The

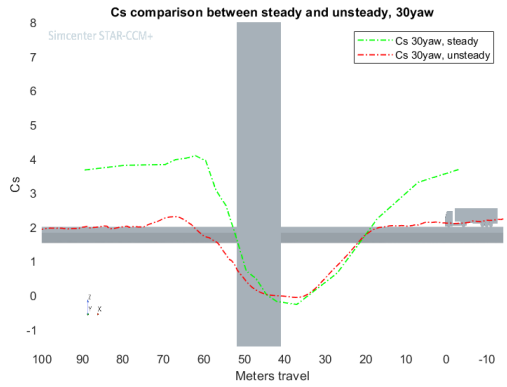

(a) Cs comparison - 30 yaw

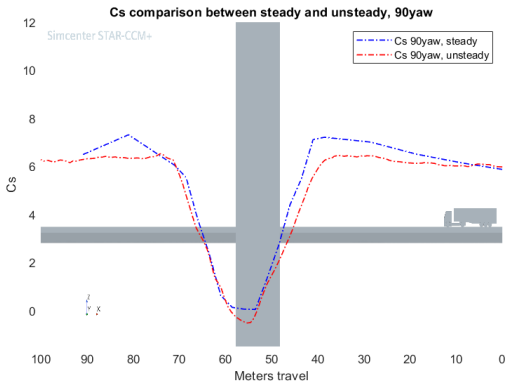

(b) Cs Comparison -90 yaw

Figure 4.39: Cs comparison between steady and unsteady simulation - 30 yaw and 90 yaw side wind condition

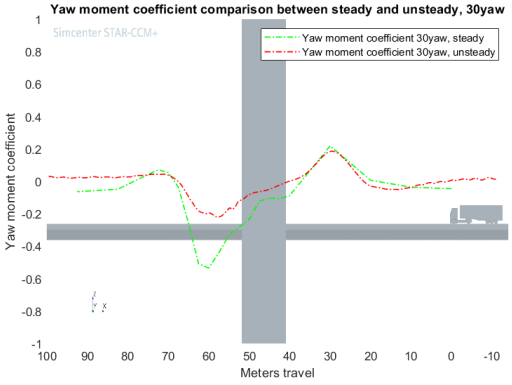

(a) Yaw moment coefficient comparison - 30 yaw

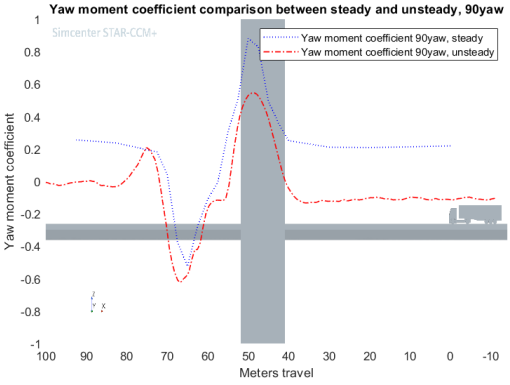

(b) Yaw moment coefficient comparison - 90 yaw

Figure 4.40: Yaw moment coefficient comparison between steady and unsteady simulation - 30 yaw and 90 yaw side wind condition

figs.4.40a and 4.40b illustrate the comparison of yaw moment coefficients. The trends correspond to 30 and 90 yaw side wind conditions.

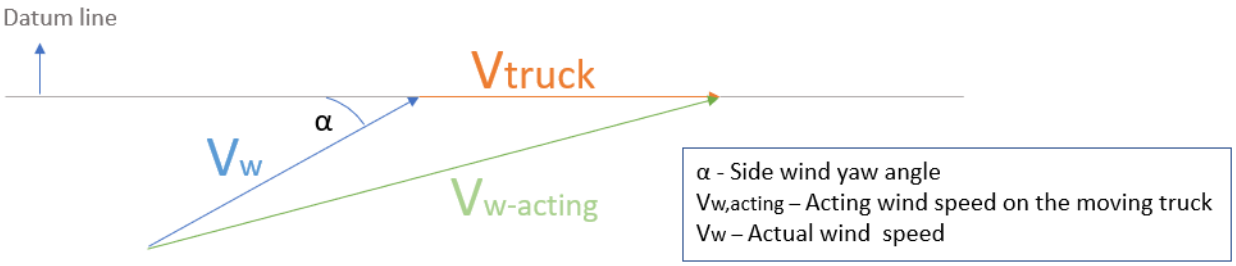

Figure 4.41: Velocity diagram for unsteady case - For a moving truck

It can be observed that, both the steady and unsteady results are fairly close to each other in the near vicinity of pylon, especially in the region of turbulent wake flow. As well, both the models are showing similar trends as illustrated by the figures.4.39 and 4.40. But, away from the pylon, the results show quite a significant difference between the steady and unsteady model. This is due to the fact that, the acting angle of attack and the resultant wind speed are different from their actual components, if the truck is in travel. This is represented in the fig.4.41. For the steady state model, the actual wind speed(V_w) is the acting wind speed($V_w, acting$) on the truck, which is stationary. As well, for the unsteady case, the NS transport equations will be solved with both the time-derivative and a spatial-derivative term. But, in the case of steady state model, the transport equations are solved only with a spatial-derivative term.

5
Conclusions

A three-dimensional CFD model was developed in this study and investigated the aerodynamic forces and moments on the truck at different side wind conditions and at different locations on the bridge. The results of both the steady and unsteady cases were compared and discussed. The major findings of the study are discussed in this chapter.

Firstly, it was realized that a good and fine mesh around the truck and pylon is very vital to resolve the gradients effectively in the wake flow and in the wake around the truck. The wake formation is highly dependent on the wind yaw angle, and hence, different meshing strategies have been adopted to solve the problem. The surface wrapper is used in conjunction with the surface remesher in the commercial code, StarCCM+, to obtain a good surface mesh. Because a good surface mesh is always required for a good volume mesh. These pre-processes yielded a stable solution, which was observed upon monitoring the side force coefficients.

Conclusions drawn from the CFD investigations with regard to individual bridge structures are:

- When compared to the case with no bridge structures, the presence of the deck alone reduced the side force acting on the vehicle by approximately 20%.
- When compared to other positions away from the pylon, the presence of the pylon generates a massive wake structure from side wind events, and this pylon wake completely shields the truck from the incoming side wind and exhibits a minimum C_S.
- The presence of windshields without cutouts reduced the side force on the truck by diverting the flow and generating a localized wake beside the exposed truck surface with minimal static pressure.
- The interaction between the stagnation regions on the exposed side of the windshield and the windward side of the truck, showed an increase in C_S, when compared versus no-shield model. This was observed for the windshields with 80% of porosity.

The steady state simulations were as well carried out for the truck at different positions on the bridge to understand the influence of the bridge structures on the forces and moments acting on the truck at every corresponding location. The obtained trend on C_s from steady state solution was analyzed in terms of its technical suitability for the given case and the flow physics. One of the main limitations of the steady state model is that the drag coefficient(C_d) on the truck was found to be negative at the location of the turbulent wake near the pylon. This is due to the fact that, the CFD investigations were carried out for the stationary truck and the flow physics with respect to the motion was not captured. In addition to this, the x-component of the velocity inlet (in the direction of truck motion)

for a 90 yaw side wind case in the simulation model is zero upon resolving the components.

With a focus to mimic the real-time scenario, the unsteady simulation model was developed. In this case, the truck motion was set for 150 meters of travel across the bridge using overset mesh methodology. This was carried out to study the dynamics of aerodynamic forces and moments on the truck in motion that commutes across the bridge pylon. The solution from the steady state simulation was used for the initialization of the unsteady model.

From the unsteady simulations, it was observed that the minimum side force on the truck was found to be at the position of the intense turbulent wake region, which is dependent on the side wind yaw angle. The maximum C_s was observed in the flow accelerated region that is in the immediate vicinity around the wake. The C_s trend exhibits continuous variation between these regions. Due to these variations, the lateral stability of the vehicle might get disturbed due to high yaw moments and this would result in maneuvering problems for the driver.

The C_s almost tended to be constant in the far-off locations away from the pylon wake on either side because there were no significant gradients in the flow-field. However, the obtained trend from this unsteady case is quite generic, as the case was modelled and analyzed with regard to the available computational resources and time. It was discussed in chapter 4 that the results on C_s from steady and unsteady models shown a difference in the obtained values at the locations away from the pylon wake. The acting angle of attack and the acting wind velocity relative to the incoming side wind yaw angle on the moving vehicle is different from the actual component. It is because of this reason, the values of the computed C_s from the unsteady model is different from the values computed through steady state simulations.

6
Future Work

As discussed in the previous chapter, this is comparatively a generic study. If the time and availability of resources were more adequate, then, it would have been ameliorated in many directions. Hence, there are quite a lot of opportunities for further research and improvements. Some of the improvement areas that are foreseen are,

- Wind tunnel tests are essential to validate the results of CFD simulations and to calibrate the computational model.
- Due to computational resources and time constraints, only 150 meters of the truck travel distance is implemented in the current unsteady model. So, scaling up the computational domain allows for a longer truck travel across the bridge deck with the truck's starting position away from the pylon wake and end boundaries. In addition to this, $DDES$ turbulence model can be implemented to study the vortex structures in the wake flows. This model as well allows the blending of $URANS$ and LES, and thus increases the resolved turbulence activity near the wall, with fine adjustments in the resolved logarithmic layer. This will yield better results on the aerodynamic forces acting on the truck, since more turbulence is resolved in this case than modelled as in $URANS$.
- In the case of a 90-degree yaw side wind, windshields with 80 percent porosity, resulted in more side force on the truck than no shields. This is due to the interaction of stagnation regions on the exposed side of the windshield and the truck. This can further be analyzed to formulate conditions on how far the truck needs to be away from the windshield to avoid the interaction of high-pressure stagnation regions.
- The concept of platooning on the bridge, vehicle over-taking, and oncoming traffic conditions can as well be investigated to understand the interaction from multiple degrees of freedom.
- The region between the accelerated flow and the pylon wake is highly dynamic and induces high yaw moments on the truck. Therefore, simulations using a driving simulator could be performed to further understand what the reactions of drivers would be in such a harsh scenario.

Bibliography

[1] Bettle, J., A. G. L. Holloway, and J. E. S. Venart. "A computational study of the aerodynamic forces acting on a tractor-trailer vehicle on a bridge in cross-wind." Journal of Wind Engineering and Industrial Aerodynamics 91.5 (2003): 573-592.

[2] Salati, L., Schito, P., Rocchi, D., Sabbioni, E. (2018). Aerodynamic study on a heavy truck passing by a bridge pylon under crosswinds using CFD. Journal of Bridge Engineering, 23(9), 04018065.

[3] Argentini., Tommaso., et al. "Cross-wind effects on a vehicle crossing the wake of a bridge pylon." Journal of wind engineering and industrial aerodynamics 99.6-7 (2011): 734-740.

[4] Tian Zang., Wei Wei Guo., Fei Duo. (2013). Effect of windproof barrier on aerodynamic performance of vehicle-bridge system. EURODYN 2017

[5] William, Y. E., Mohamed, M. H., Oraby, W. A. (2013). Investigation of Crosswind Aerodynamics for Road Vehicles Using CFD Technique. In Eleventh International Conference of Fluid Dynamics (pp. 19-21)

[6] Siemens, The Steve Portal, Guidelines for Star CCM+ by Siemens, https://support.sw.siemens.com/en-US/product/226870983

[7] Chen, Ning, et al. "Effects of wind barrier on the safety of vehicles driven on bridges." Journal of Wind Engineering and Industrial Aerodynamics 143 (2015): 113-127.

[8] Xiang, H., Li, Y., Chen, S., Hou, G. (2018). Wind loads of moving vehicle on bridge with solid wind barrier. Engineering structures, 156, 188-196.

[9] Wang, Bin, et al. "Determination of aerodynamic forces on stationary/moving vehicle-bridge deck system under crosswinds using computational fluid dynamics." Engineering Applications of Computational Fluid Mechanics 7.3 (2013): 355-368.

DEPARTMENT OF MECHANICS AND MARITIME SCIENCES
CHALMERS UNIVERSITY OF TECHNOLOGY
Gothenburg, Sweden
www.chalmers.se

CHALMERS
UNIVERSITY OF TECHNOLOGY